Figure 4. Alveolar bone regeneration following the transplantation of a bioengineered tooth unit. (A) Schematic representation of a murine extensive bone defect model and the transplantation of a bioengineered tooth unit (arrowhead). (B) Micro-CT images of the vertical alveolar bone regeneration processes in a no transplantation control (*upper*) and following the transplantation of a bioengineered tooth unit (arrowhead, *lower*) in a murine extensive bone defect model. Vertical bone formation was observed from the marginal bone of the recipient (arrow). Scale bar, 500 μm. (C) Three-dimensional superposition of micro-CT images of natural dentition (gray, double dotted line), a transplanted bioengineered tooth unit (*lower*) and a no transplantation control (*upper*) at day 0 in an extensive bone defect (red, straight line), and at 45 days after transplantation (green, dotted line). The superior edges of the recipient alveolar bone are indicated by each line. (D) Regenerative bone volume of the buccal area following the transplantation of a bioengineered tooth unit (transplant) and no transplantation (control) at day 45 in an extensive bone defect. Error bars show the standard deviation ($n = 4$). *$P < 0.01$ (t-test).
doi:10.1371/journal.pone.0021531.g004

therapies with BMPs, FGFs or PDGF, no clinical protocol for bone regeneration in the vertical and horizontal dimensions has been established yet [31]. In our present study however, we demonstrate that a bioengineered tooth unit could be engrafted and integrate via recipient bone remodeling after transplantation into an extensive bone defect. The recipient alveolar bone of the vertical dimension was observed to maintain the height of the PDL in the bioengineered tooth unit. These findings indicate that the transplantation of a bioengineered tooth has great potential for not only future whole tooth regenerative therapy but also as a treatment in clinical cases where tooth loss is accompanied by a serious alveolar bone defect.

Further studies of three-dimensional organ culture technologies *in vitro*, which can generate a fully functional bioengineered organ, and the identification of available adult tissue stem cells for the reconstitution of a bioengineered tooth germ will be required in the future to realize whole tooth regenerative therapy in the clinic.

Materials and Methods

Ethics Statement

All animals and experimental protocols were approved by the Tokyo University of Science Animal Care and Use Committee (Permit Number: N10018). All surgery was performed under sodium pentobarbital anesthesia, and all efforts were made to minimize suffering.

Reconstitution of a bioengineered tooth germ from single cells

Molar tooth germs were dissected from the mandibles of ED14.5 mice. The isolation of tissues and single cell preparations from the epithelium and mesenchyme has been described previously [22]. Dissociated epithelial and mesenchymal cells were precipitated by centrifugation in a siliconized microtube and the supernatant was completely removed. The cell density of the precipitated epithelial and mesenchymal cells after the removal of the supernatants reached a concentration of 5×10^8 cells/ml [22]. Bioengineered molar tooth germ was reconstituted using our previously described 3-dimensional cell manipulation technique, the organ germ method [22]. We used 5×10^4 epithelial and mesenchymal cells each to generate single tooth structures. The bioengineered tooth germs were incubated for 10 min at 37°C, placed on a cell culture insert (0.4 μm pore diameter; BD, Franklin Lakes, New Jersey, USA), and then further incubated at 37°C for five days in an *in vitro* organ culture as described previously [22].

Generation of a bioengineered tooth unit

To control the length and shape of the bioengineered tooth unit, we manufactured a plastic ring-shaped structure, which was used as a size-control device, of a 1.3, 1.8 or 2.5 mm inside diameter and 1.3 mm thickness. After five days of cultivation, the reconstituted tooth germs were placed into this spacing device which was transplanted into a subrenal capsule for 60 days using 7-week-old female mice as the hosts. The bioengineered tooth unit was then isolated from the device.

Fluorescent calcein labeling

Calcein (Wako, Osaka, Japan) was administered daily (1.6 mg/kg) via a subcutaneous dose to the transplanted bioengineered tooth germ in the subrenal capsule. These tooth units were then transplanted into the extracted regions of a lower first molar for 14, 30 or 40 days. Non-decalcified frozen sections were then prepared and observed using an Axiovert (Carl Zeiss, Oberkochen, Germany) with AxioCAM MRc5 (Carl Zeiss).

Transplantation

The lower first molars of 4-week-old C57BL/6 (SLC, Shizuoka, Japan) mice were extracted under deep anesthesia and the resulting gingival wounds had been allowed to heal for 4–6 days. The transplantation of a bioengineered tooth unit was allowed the procedure as described previously [20]. To generate an extensive alveolar bone defect mouse model, the whole supporting alveolar bone (1.5 mm mesiodistally, 1.2 mm buccolingually and 0.6 mm vertically) was removed using a dental engine (NSK, Tochigi, Japan) under deep anesthesia. The bioengineered tooth units were transplanted into these defects using the same procedure described above.

Microcomputed Tomography (Micro-CT)

The heads of the mice that had received a transplanted bioengineered tooth unit and normal mice were arranged in the centric occlusal position and radiographic imaging was then performed by x-ray using a Micro-CT device (R_mCT; Rigaku, Tokyo, Japan) with exposure at 90 kV and 150 mA. Micro-CT images were captured using i-view R (Morita, Kyoto, Japan) and Imaris (Carl Zeiss).

Histochemical analysis and immunohistochemistry

Histochemical and immunohistochemical tissue analyses were performed as described previously [20,22].

Hardness measurements

Polished enamel and dentin samples from bioengineered tooth units extracted at 60 days after germ transplantation into the SRC or the mandible, and also a normal tooth (9-week postnatal) were embedded in acrylic resin (n = 5 for each group). The Knoop hardness test was then performed using a Miniload Hardness Tester (HM-102; Mitutoyo, Kanagawa, Japan) equipped with a Knoop diamond tip (19BAA061; Mitutoyo). Five indentations were made on each specimen with a 10 g load for 10 sec.

Experimental orthodontic treatments

Orthodontic treatment was performed as described previously [20]. Experimental tooth movements consisted of a horizontal orthodontic force of about 10–15 g applied continuously to the bioengineered tooth of the mice in the experimental group in a buccal direction using a dial tension gauge (Mitutoyo) for six days. In the control group, orthodontic force was applied in the buccal direction to the first molars of 7-week-old normal C57BL/6 mice in the same manner as the experimental group. Serial sections at day 6 were analyzed by TRAP staining and by *in situ* hybridization analysis for osteocalcin (*Ocn*) mRNA as previously described [20].

Pulp exposure

A minimal pinpoint mechanical exposure of the pulp was made in the bioengineered tooth or control natural first molar of mice under anesthesia using a dental engine (NSK) supplied with dental diamond point (Shofu, Kyoto, Japan). For stimulation with cold water, ice was applied to the cavity of the tooth after pulp exposure.

Measurement of the regenerative bone volume

To evaluate the extent of the alveolar bone recovery in our extensive bone defect mouse model, we used the Micro-CT device (Rigaku) to measure alveolar bone volume of the treated areas at 0 and 45 days after transplantation. We measured the volume of the alveolar bone in the operated region using TRI/3D-BON software (Ratoc, Osaka, Japan). The 3D region of interest (ROI)

was selected in the buccal alveolar bone area which was prescribed from the medial edge of lower second molar to the distal edge of the foramen mentale. We subtracted the alveolar bone volume of the area at day 0 from the volume at day 45, and calculated the regenerated bone volume.

Statistical analysis

Statistical significance was determined with the unpaired Student's t-test, analyzed using the Common Gateway Interface Program (twk, Saint John's University).

Supporting Information

Figure S1 A method for controlling the size of a bioengineered tooth unit. (A) Micro-CT images of the shapes of a bioengineered tooth unit, size controlled by devices of a 1.3 or 1.8 mm inner diameter, at 30 and 60 days after transplantation in an SRC. Scale bar, 500 μm. (B) Photograph of plural bioengineered tooth germ arranged in a size controlled device. Scale bar, 500 μm. (C) Micro-CT images (*left*) and histological analysis of the multiple bioengineered tooth units on day 60 after SRC transplantation (*middle and right*). The alveolar bone between the bioengineered teeth is indicated by arrowheads (*lower left*). Scale bar, 200 μm. Higher magnification images of the periodontal tissue area (*lower middle and right*) are also shown. Scale bar, 50 μm. D, dentin; AB, alveolar bone; PDL, periodontal ligament. (TIF)

Figure S2 Engraftment and establishment of occlusion of a bioengineered tooth unit at the tooth loss region. (A) Oral photographs and micro-CT images of bioengineered tooth unit transplantations into the adult mandible. Images were captured of lateral (*top*), occlusal (*middle*) and cross sections (*bottom*) views. The bioengineered tooth unit is indicated by an arrowhead. Scale bar, 500 μm. (B) Sectional images of a calcein-labeled bioengineered tooth unit at 14, 30 and 40 days after transplantation into a murine model. Fluorescent and DIC images are merged. The alveolar bone of the bioengineered tooth unit is indicated by arrowheads. Scale bar, 500 μm, *upper*; 100 μm, *lower*. NT, natural tooth; BT, bioengineered tooth. (C) Oral photographs of an engrafted bioengineered tooth in a lateral view (upper left), a 45-degree view (*lower left*), an occlusal view (*upper right*) and a fluorescent image (*lower right*). Scale bar, 500 μm. (D) Measurements of the tooth length (*left*) and apical foramen width (*right*) of a bioengineered tooth at day 0 and day 40 after transplantation. Error bars show the standard deviation ($n = 9$). *$P < 0.05$ (t-test). (E) Schematic representation of the protocol for transplanting multiple bioengineered tooth units in a murine edentulous model. (F) Micro-CT images of transplanted multiple bioengineered tooth

units in a murine edentulous model. Images were captured of the external surface area (*left*), sagittal section (*center*) and cross section (*right*). The bioengineered teeth are indicated by the arrowheads in the left figure. Scale bar, 500 μm. (TIF)

Figure S3 Regeneration of nerve fibers and blood vessels in the engrafted bioengineered tooth unit. (A, B) Nerve fibers and blood vessels in the pulp (A) and PDL (B) of a natural tooth (*top*), bioengineered tooth unit in an SRC (*middle*) and bioengineered tooth at 40 days after transplantation into an oral tooth loss region (*bottom*) were analyzed immunohistochemically using specific antibodies for NF and vWF. DIC (*first columns from the left*), NF images (*second columns*), vWF images (*third columns*), and merged images (*fourth columns*) are shown. Scale bar, 50 μm. (C, D) Nerve fibers in the pulp (C) and PDL (D) of a natural tooth (*top*), bioengineered tooth unit in an SRC (*middle*) and bioengineered tooth at 40 days after transplantation (*bottom*) were analyzed immunohistochemically using specific antibodies for NF and neuropeptide Y (NPY). DIC (*first columns from the left*), NF images (*second columns*), NPY images (*third columns*), and merged images (*fourth columns*) are shown. Scale bar, 50 μm. (E, F) Nerve fibers in the pulp (E) and PDL (F) of a natural tooth (*top*), bioengineered tooth unit in an SRC (*middle*) and bioengineered tooth at 40 days after transplantation (*bottom*) were analyzed immunohistochemically using specific antibodies for NF and calcitonin gene-related peptide (CGRP). DIC (*first columns from the left*), NF images (*second columns*), CGRP images (*third columns*), and merged images (*fourth columns*) are shown. Scale bar, 50 μm. (TIF)

Figure S4 Alveolar bone regenerative potential of a bioengineered tooth unit. (A) Photographs of a lateral (*left*) and occlusal (*right*) view of a natural mandibular dentition and an extensive bone defect (arrowhead). Scale bar, 500 μm. (B) Micro-CT images of the frontal section of a no transplantation control (*upper*) and a transplanted bioengineered tooth unit at day 45 in a murine extensive bone defect model (*lower*). Significant vertical bone regeneration was observed following the transplantation of a bioengineered tooth unit when compared with the no transplantation control. The regenerated alveolar bone is indicated by an arrow. Scale bar, 500 μm. (TIF)

Author Contributions

References

1. Lechler RJ, Sykes M, Thomson AW, Turka LA (2005) Organ transplantation-how much of the promise has been realized? Nat Med 11: 605-613.
2. Gridelli B, Remuzzi G (2000) Strategies for making more organs available for transplantation. N Engl J Med 343: 404-410.
3. Moers C, Smits JM, Maathuis MH, Treckmann J, van Gelder F. et al. (2009) Machine perfusion or cold storage in deceased-donor kidney transplantation. N Engl J Med 360: 7-19.
4. Copelan EA (2006) Hematopoietic stem-cell transplantation. N Engl J Med 354: 1813-1826.
5. Nishikawa S, Goldstein RA, Nierras CR (2008) The promise of human induced pluripotent stem cells for research and therapy. Nat Rev Mol Cell Biol 9: 725-729.
6. Miyahara Y, Nagaya N, Kataoka M, Yanagawa B, Tanaka K, et al. (2006) Monolayered mesenchymal stem cells repair scarred myocardium after myocardial infarction. Nat Med 12: 459-465.
7. Ohashi K, Yokoyama T. Yamato M, Kuge H, Kanehiro H, et al. (2007) Engineering functional two- and three-dimensional liver systems in vivo using hepatic tissue sheets. Nat Med 13: 880-885.
8. Korbling M, Estrov Z (2003) Adult stem cells for tissue repair - a new therapeutic concept? N Engl J Med 349: 570-582.
9. Atala A (2005) Tissue engineering, stem cells and cloning: current concepts and changing trends. Expert Opin Biol Ther 5: 879-892.
10. Purnell B (2008) New release: the complete guide to organ repair. Introduction Science 322: 1489.
11. Ikeda E, Tsuji T (2008) Growing bioengineered teeth from single cells: potential for dental regenerative medicine. Expert Opin Biol Ther 8: 735-744.
12. Layer PG, Robitzki A, Rothermel A, Willbold E (2002) Of layers and spheres: the reaggregate approach in tissue engineering. Trends Neurosci 25: 131-134.
13. Yelick PC, Vacanti JP (2006) Bioengineered teeth from tooth bud cells. Dent Clin North Am 50: 191-203, viii.
14. Khademhosseini A, Langer R, Borenstein J, Vacanti JP (2006) Microscale technologies for tissue engineering and biology. Proc Natl Acad Sci U S A 103: 2480-2487.
15. Uygun BE, Soto-Gutierrez A, Yagi H, Izamis ML, Guzzardi MA, et al. (2010) Organ reengineering through development of a transplantable recellularized liver graft using decellularized liver matrix. Nat Med 16: 814-820.

16. Zheng Y, Du X, Wang W, Boucher M, Parimoo S, et al. (2005) Organogenesis from dissociated cells: generation of mature cycling hair follicles from skin-derived cells. J Invest Dermatol 124: 867–876.

17. Shackleton M, Vaillant F, Simpson KJ, Stingl J, Smyth GK, et al. (2006) Generation of a functional mammary gland from a single stem cell. Nature 439: 84–88.

18. Yen AH, Sharpe PT (2006) Regeneration of teeth using stem cell-based tissue engineering. Expert Opin Biol Ther 6: 9–16.

19. Sharpe PT, Young CS (2005) Test-tube teeth. Sci Am 293: 34–41.

20. Ikeda E, Morita R, Nakao K, Ishida K, Nakamura T, et al. (2009) Fully functional bioengineered tooth replacement as an organ replacement therapy. Proc Natl Acad Sci U S A 106: 13475–13480.

21. Nickel JC, Iwasaki LR, Walker RD, McLachlan KR, McCall WD, Jr. (2003) Human masticatory muscle forces during static biting. J Dent Res 82: 212–217.

22. Nakao K, Morita R, Saji Y, Ishida K, Tomita Y, et al. (2007) The development of a bioengineered organ germ method. Nat Methods 4: 227–230.

23. Zaret KS, Grompe M (2008) Generation and regeneration of cells of the liver and pancreas. Science 322: 1490–1494.

24. Slack JM (2008) Origin of stem cells in organogenesis. Science 322: 1498–1501.

25. Hu B, Nadiri A, Kuchler-Bopp S, Perrin-Schmitt F, Peters H, et al. (2006) Tissue engineering of tooth crown, root, and periodontium. Tissue Eng 12: 2069–2075.

26. Van der Weijden F, Dell'Acqua F, Slot DE (2009) Alveolar bone dimensional changes of post-extraction sockets in humans: a systematic review. J Clin Periodontol 36: 1048–1058.

27. Wang X, Yan Y, Zhang R (2010) Recent trends and challenges in complex organ manufacturing. Tissue Eng Part B Rev 16: 189–197.

28. Ishida K, Murofushi M, Nakao K, Morita R, Ogawa M, et al. (2011) The regulation of tooth morphogenesis is associated with epithelial cell proliferation and the expression of Sonic hedgehog through epithelial-mesenchymal interactions. Biochem Biophys Res Commun 405: 455–461.

29. Geertman ME, Slagter AP, van Waas MA, Kalk W (1994) Comminution of food with mandibular implant-retained overdentures. J Dent Res 73: 1858–1864.

30. Byers MR, Narhi MV (1999) Dental injury models: experimental tools for understanding neuroinflammatory interactions and polymodal nociceptor functions. Crit Rev Oral Biol Med 10: 4–39.

31. Bueno EM, Glowacki J (2009) Cell-free and cell-based approaches for bone regeneration. Nat Rev Rheumatol 5: 685–697.

32. Kinoshita M, Ariizumi T, Yuasa S, Miyoshi S, Komazaki S, et al. (2010) Creating frog heart as an organ: in vitro-induced heart functions as a circulatory organ in vivo. Int J Dev Biol 54: 851–856.

33. Sedohara A, Komazaki S, Asashima M (2003) In vitro induction and transplantation of eye during early Xenopus development. Dev Growth Differ 45: 463–471.

34. Tyler D, Baker NE (2003) Size isn't everything. Bioessays 25: 5–8.

35. Cai J, Cho SW, Kim JY, Lee MJ, Cha YG, et al. (2007) Patterning the size and number of tooth and its cusps. Dev Biol 304: 499–507.

36. Jernvall J, Thesleff I (2000) Reiterative signaling and patterning during mammalian tooth morphogenesis. Mech Dev 92: 19–29.

37. Kallu R, Vinckier F, Politis C, Mwalili S, Willems G (2005) Tooth transplantations: a descriptive retrospective study. Int J Oral Maxillofac Surg 34: 745–755.

38. Cho MI, Garant PR (2000) Development and general structure of the periodontium. Periodontol 2000 24: 9–27.

ADAMTSL6β Protein Rescues Fibrillin-1 Microfibril Disorder in a Marfan Syndrome Mouse Model through the Promotion of Fibrillin-1 Assembly*[S]

Masahiro Saito,[a,b1] Misaki Kurokawa,[a] Masahito Oda,[a] Masamitsu Oshima,[b] Ko Tsutsui,[d] Kazutaka Kosaka,[e]
Kazuhisa Nakao,[b] Miho Ogawa,[b,c] Ri-ichiroh Manabe,[f] Naoto Suda,[g] Ganburged Ganjargal,[g] Yasunobu Hada,[a,h]
Toshihide Noguchi,[i] Toshio Teranaka,[e] Kiyotoshi Sekiguchi,[d] Toshiyuki Yoneda,[j] and Takashi Tsuji[a,b,c]

From the [a]Department of Biological Science and Technology, Faculty of Industrial Science and [b]Research Institute for Science and
Technology, Tokyo University of Science, Noda, Chiba 278-8510, Japan, [c]Organ Technologies Inc., Tokyo, Japan, the [j]Department
of Molecular and Cellular Biochemistry, Graduate School of Dentistry, and the [d]Institute for Protein Research, Osaka University,
Suita Osaka 565-0871, Japan, the [e]Division of Restorative Dentistry, Department of Oral Medicine, Kanagawa Dental College,
Yokosuka Kanagawa 238-8580, Japan, the [i]Department of Periodontology, School of Dentistry, Aichi-Gakuin University, Nisshin
470-0195, Japan, [g]Maxillofacial Orthognathics and [h]Oral Implantology and Regenerative Dental Medicine, Graduate School,
Tokyo Medical and Dental University, Tokyo 113-0034, Japan, and the [f]RIKEN Genomic Sciences Center, RIKEN Yokohama Institute,
Yokohama 230-0045, Japan

Background: The pathology of Marfan syndrome is caused by insufficient fibrillin-1 microfibril formation in connective tissues.

Results: Successful improvement of Marfan syndrome manifestations are induced by the direct administration of recombinant ADAMTSL6β.

Conclusion: This study demonstrated critical importance of microfibril regeneration in preventing Marfan syndrome.

Significance: Our current data support a new concept that the regeneration of microfibrils using ADAMTSL6β is essential for improving Marfan syndrome.

Marfan syndrome (MFS) is a systemic disorder of the connective tissues caused by insufficient fibrillin-1 microfibril formation and can cause cardiac complications, emphysema, ocular lens dislocation, and severe periodontal disease. ADAMTSL6β (A disintegrin-like metalloprotease domain with thrombospondin type I motifs-like 6β) is a microfibril-associated extracellular matrix protein expressed in various connective tissues that has been implicated in fibrillin-1 microfibril assembly. We here report that ADAMTSL6β plays an essential role in the development and regeneration of connective tissues. ADAMTSL6β expression rescues microfibril disorder after periodontal ligament injury in an MFS mouse model through the promotion of fibrillin-1 microfibril assembly. In addition, improved fibrillin-1 assembly in MFS mice following the administration of ADAMTSL6β attenuates the overactivation of TGF-β signals associated with the increased release of active TGF-β from disrupted fibrillin-1 microfibrils within periodontal ligaments. Our current data thus demonstrate the essential contribution of ADAMTSL6β to fibrillin-1 microfibril formation. These findings also suggest a new therapeutic strategy for the treatment of MFS through ADAMTSL6β-mediated fibrillin-1 microfibril assembly.

Marfan syndrome (MFS)[2] is a severe, systemic disorder of connective tissue formation and can lead to aortic aneurysms, ocular lens dislocation, emphysema, bone overgrowth, and severe periodontal disease (1–3). MFS has an estimated prevalence of 1 in 5,000–10,000 individuals (3, 4). Fibrillin-1 comprises one of the major insoluble extracellular matrix components in connective tissue microfibrils and provides limited elasticity to tissues through fibrillin-1 microfibril formation (5, 6). Various mouse models of MFS have been established via gene targeting or missense mutations, with germ line mutations in fibrillin-1 leading to progressive connective tissue destruction due to fibrillin-1 fragmentation in association with an insufficiency of fibrillin-1 microfibril formation (7–10). Hence, it is largely accepted that MFS is caused by insufficient fibrillin-1 microfibril formation in various connective tissues (11, 12).

A variety of MFS therapies have been developed, including surgical therapy for aortic root aneurysms that are life-threatening (12), traditional medical therapies, such as β-adrenergic receptor blockade, for slow aortic growth and to decrease the risk of aortic dissection, and novel approaches based on new insights, such as the pathogenesis of insufficient fibrillin-1

microfibril formation and deregulation of TGF-β activation (2). It has been demonstrated also that deregulation of TGF-β activation contributes to MFS pathogenesis and that matrix sequestration of TGF-β is critical for the regulated activation and signaling of the extracellular fibrillin-1 microfibrils of connective tissues (8). These observations predict that the clinical features of MFS-like manifestations are caused by alterations in TGF-β signaling networks (13). Loeys-Dietz syndrome, which is caused by heterozygous mutations in the genes encoding TGF-β receptors 1 and 2, is another autosomal dominant disorder with MFS-like manifestations, such as aortic root aneurysms, aneurysms and dissections throughout the arterial tree, and generalized arterial tortuosity (4). Importantly, systemic antagonism of TGF-β signaling through the administration of a TGF-β-neutralizing antibody or losartan, an angiotensin II type 1 receptor blocker, has been shown to have a beneficial effect on alveolar septation and muscle hypoplasia (8, 10). These observations provide a proof of principle for the use of TGF-β antagonism is in a general therapeutic strategy for MFS and other disorders of the TGF-β signaling network. However, another potential therapeutic strategy that remains to be investigated is the reconstruction of the microfibril in connective tissues through the expression or administration of a microfibril-associated molecule that regulates or stabilizes fibrillin-1 microfibril formation. To investigate this concept, it will be necessary to identify molecular mechanisms of microfibril formation and an appropriate fibrillin-1 microfibril-associated molecule.

ADAMTSL (A disintegrin-like metalloprotease domain with thrombospondin type I motifs-like) is a subgroup of the ADAMTS superfamily that shares particular protein domains with the ADAMTS protease, including thrombospondin type I repeats, a cysteine-rich domain, and an ADAMTS spacer, but lacks the catalytic and disintegrin-like domains (14). A recent study has demonstrated that ADAMTSL2 mutations cause geleophysic dysplasia, an autosomal recessive disorder similar to MFS, through the dysregulation of TGF-β signaling (15). A homozygous mutation in ADAMTSL4 also causes autosomal recessive isolated ectopia lentis, another disease similar to MFS that is characterized by the subluxation of the lens as a result of disruption of the zonular fibers (16). The novel ADAMTSL family molecules ADAMTSL6α and -6β were recently identified by *in silico* screening for novel ECM proteins produced from a mouse full-length cDNA data base (FANTOM). These proteins are localized in connective tissues, including the skin, aorta, and perichondrocytes. Among the ADAMTSL6 family, ADAMTSL6β has been shown to associate with fibrillin-1 microfibrils through its direct interaction with the N-terminal region of fibrillin-1 and thereby promotes fibrillin-1 matrix assembly *in vitro* and *in vivo* (17). These findings suggest a potential clinical application of ADAMTSL6β as a novel MFS therapy by promoting fibrillin-1 microfibril assembly and regulating TGF-β activation.

In our current study, we report that ADAMSL6β is essential for the development and regeneration of the connective tissue periodontal ligament (PDL), a tooth-supporting tissue located between the root and alveolar bone that is morphologically similar to the ligament tissue that is capable of withstanding mechanical force. Using mgR/mgR mice as an animal model of

MFS microfibril disorder, we demonstrate that ADAMSL6β expression can rescue fibrillin-1 microfibril formation through the promotion of fibrillin-1 microfibril assembly. PDL provides a useful experimental model not only for investigating the molecular pathogenesis of MFS but also for evaluating novel therapeutic strategies for the improvement of microfibril disorders. This is because the principal elastic fiber system of PDL is composed of fibrillin-1 microfibrils and does not contain significant amounts of elastin (18–20). This composition also suggests that PDL will have an increased susceptibility to breakdown in MFS compared with other elastic tissues composed of both elastin and fibrillin-1. Furthermore, the restoration of fibrillin-1 assembly following administration of recombinant ADAMTSL6β regulates the overactivation of TGF-β signaling, which is associated with an increased release of active TGF-β from disrupted fibrillin-1 microfibrils. The results of our present study demonstrate for the first time that ADAMTSL6β is essential for fibrillin-1 microfibril formation and suggest a novel therapeutic approach to the treatment of MFS through the promotion of ADAMTSL6β-mediated fibrillin-1 microfibril assembly.

EXPERIMENTAL PROCEDURES

Animals—C57BL/6 mice were purchased from CLEA Japan, Inc. (Tokyo, Japan). mgR/mgR mice were generously provided by Dr. Francesco Ramirez (Mount Sinai Medical Center, New York). All mouse care and handling conformed to the National Institutes of Health guidelines for animal research. All experimental protocols were approved by the Tokyo University of Science Animal Care and Use Committee.

Histochemical Analysis—Frontal sections of C57BL mouse heads at embryonic day 13 (E13), E15, E17, and postnatal day 1 (P1) were prepared as described above. Fresh frozen sections of P7 and P35 mice were prepared using the Kawamoto tape method, according to the manufacturer's instructions (Leica Microsystems, Tokyo, Japan) (21), and 10-μm sagittal sections were generated. Cells were fixed with 4% paraformaldehyde and blocked with 1% BSA. The primary antibody used was an anti-Adamtsl6 polyclonal antibody (R1–1) (17), anti-fibrillin-1 polyclonal antibody (pAB9543), anti-FIBRILLIN-1 monoclonal antibody (clone 69, Chemicon, Temecula, CA), and anti-FLAG M2 monoclonal antibody (Sigma-Aldrich). The secondary antibodies used were Alexa 488 or Alexa 555 anti-rabbit or anti-mouse IgG (Invitrogen), followed by nuclear staining with DAPI. An anti-Adamtsl6 polyclonal antibody was labeled with Alexa 488 by using the Zenon antibody labeling kit according to the manufacturer's instructions (Invitrogen) for double immunostaining with an anti-fibrillin-1 polyclonal antibody. For visualization of oxytalan fibers, sections were oxidized for 15 min in 10% Oxone (Merck) and subsequently stained with aldehyde fuchsin as described previously (20). Fluorescence images were sequentially collected using a confocal microscope featuring 403-, 488-, and 543-nm laser lines (LSM510; Carl Zeiss MicroImaging, Jena, Germany). The *in situ* hybridization methodology and probe design are described in the supporting information.

ADAMTSL6β cDNA—As described previously (17), *ADAMTSL6β* or *Adamtsl6β* was cloned into p3XFLAG-

CMV-14 to generate p3XFLAG-CMV-*ADAMTSL6β*. The coding sequence of the cDNA was confirmed to be identical to the published sequence. The *ADAMTSL6β* coding sequence containing the Kozak consensus sequence and tagged with the FLAG epitope at its C terminus end was then subcloned into the pcDNA4 expression vector (Invitrogen) or into the pDONR221 vector via a BP reaction (Invitrogen) to generate adenovirus or lentivirus, respectively.

Generation of Adenovirus—Recombinant adenovirus was constructed by homologous recombination between the expression cosmid cassette (pAxCAwt) and the parental virus genome in 293 cells (Riken, Tsukuba, Japan) as described previously (22) using an adenovirus construction kit (Takara, Ohtsu, Japan).

Generation of Lentivirus—Recombinant lentivirus carrying *ADAMTSL6β* was constructed via the recombination of pDONR221-containing *ADAMTSL6β* segments into CSII-CMV-RfA using a LR reaction to generate CSII-CMV-*ADAMTSL6β*. CSII-CMV-RfA was kindly provided by Dr. Hiroyuki Miyoshi (Riken, Tsukuba, Japan). Lentiviruses were produced essentially as described previously (23). Next, a 500-μl aliquot of producer cell culture fluid was added to human periodontal ligament (HPDL) (passage 7) or MFS periodontal ligament (MHPDL) (passage 7) cells in the presence of Polybrene (7.5 μg/ml). Stably transduced cells were maintained in the medium described above.

For knockdown experiments, miRNA expression vectors were constructed according to the manufacturer's protocol (Invitrogen). Two sets of Adamtsl6β miRNAs to target sense (5'-TGCTGAATAACAGGTAGCTGACAAACGTTTTGGC-CACTGACTGACGTTTGTCATACCTGTTATT-3') and antisense (5'-CCTGAATAACAGGTATGACAAACGTCAG-TCAGTGGCCAAAACGTTTGTCAGCTACCTGTTATTC-3') transcripts were used to generate lentiviruses for the knockdown of Adamtsl6β. A control miRNA was purchased from Invitrogen.

Infection of Developing Tooth Germ with Adenovirus—To investigate the effects of Adamtsl6β on PDL formation in mgR/mgR mice, developing tooth germs were dissected from E14.5 mgR/mgR mouse embryos as described above and then infected with adenovirus that had been concentrated using the Adeno-X Maxi purification kit (Clontech) at 4 °C for 48 h in accordance with the manufacturer's recommendations. The adenovirus-infected tooth germs were then further incubated at 37 °C for 6 days in an *in vitro* organ culture as described previously (24).

Expression and Purification of Recombinant Adamtsl6β—The expression and purification of recombinant Adamtsl6β was performed using 293F cells (Invitrogen) and nickel-agarose (Qiagen, Hilden, Germany) as described previously (17). Briefly, pSecTag2A containing an *Adamtsl6β* segment fused with Myc and His tags at its C terminus was transfected into 293F cells, which were cultured for 3 days. Conditioned medium was applied to a nickel-agarose column for the purification of recombinant Adamtsl6β. The purified protein was dialyzed against PBS and stored at −80 °C.

Tissue Culture and in Vitro Microfibril Assembly Assay—The establishment of immortalized human periodontal cells and

MHPDL cells has been described previously (25). Cells were incubated with α-minimum essential medium (Sigma) containing 10% fetal bovine serum (FBS; BioWhittaker, Walkersville, MD), 50 μg/ml ascorbic acid, and 100 units/ml streptomycin and penicillin in a humidified atmosphere of 5% CO_2 at 37 °C. HPDL or MHPDL cells were plated onto 12-mm-thick coverglass coated with poly-L-Lys (Iwaki, Tokyo, Japan) placed in 24-well plates at 6 × 10⁴ cells/well and incubated for 14 days. For the addition of purified recombinant mouse Adamtsl6β, C-terminal histidine-tagged mouse Adamtsl6β was prepared as described previously (17). Adamtsl6β protein (10, 5, 2.5, 1.25, or 0.625 μg) and the cells were incubated for 3 days. The cells were fixed with 4% paraformaldehyde and immunostained as described above.

RNA Preparation and Real-time RT-PCR—Total RNA was isolated from cells using Isogen (Nippon Gene Co., Ltd., Tokyo, Japan) as described previously (26). cDNAs were synthesized from 1-μg aliquots of total RNA in a 20-μl reaction containing 10× reaction buffer, 1 mM dNTP mixture, 1 unit/μl RNase inhibitor, 0.25 unit/μl reverse transcriptase (M-MLV reverse transcriptase; Invitrogen), and 0.125 μM random 9-mers (Takara, Tokyo, Japan). The mRNA expression levels were determined using *Power* SYBR® Green PCR Master Mix (Applied Biosystems), and products were analyzed with an AB 7300 real-time PCR system (Applied Biosystems). Specific primers for human fibrillin-1 (forward, 5'-AATGAGCT-GAATGGCTGTTACAA-3'; reverse, 5'-ACCATATGCTA-TATATTCTTCGATAACAAT-3'), mouse fibrillin-1 (forward, 5'-AAGGGGTTAATGTCATGATGTCAC-3'; reverse, 5'-CCACACAAGAACATAAAACCAAGG-3'), and mouse glyceraldehyde-3-phosphate dehydrogenase (*GAPDH*) (forward, 5'-ACTGAGCAAGAGAGGCCCTATCC-3'; reverse, 5'-CCTAGGCCCCTCCTGTTATTATGG-3') were used for real-time PCR. The primers for human *GAPDH* have been described previously (27).

Pull-down Assay—Pull-down assays to demonstrate direct interactions between Adamtsl6β and TGF-β1 proteins were performed as described previously by Nakajima *et al.* (28). Briefly, purified recombinant mouse Adamtsl6β (5 μg) was incubated with 0.1 μg of recombinant TGF-β1 proteins (Wako, Osaka, Japan) for 1 h at 4 °C in 0.3 ml of binding buffer (20 mM Tris-HCl (pH 7.5), 150 mM NaCl, and 1% Triton X-100). We next added 12.5 μl of nickel-magnet (Promega, Madison, WI) to the reactions and incubated them for 30 min at 25 °C. The precipitates were washed three times with binding buffer, eluted by 250 mM imidazole, and subjected to SDS-PAGE. The proteins were blotted and visualized with the corresponding antibody.

Cell Culture—The method used to culture the mouse dental follicle cells has been described previously (29). To examine the effects of Adamtsl6β upon the TGF-β1-induced expression of periostin, mouse dental follicle cells were cultured in a 12-well plate at a density of 5 × 10⁴ cells/well in Dulbecco's modified Eagle's medium (DMEM) containing 10% FBS until they reached confluence. At this point, the medium was replaced with DMEM containing 0.2% FBS. After 12 h, the cells were treated with recombinant mouse Adamtsl6β. After 12 h, the

cells were treated with TGF-β1 (10 ng/ml) for 3 days and subjected to real-time PCR analysis.

Tooth Replantation Model—The tooth replantation experiments were performed as described previously (30). Briefly, the upper first molar from 4-week-old C57BL/6(SLC) mice was extracted under deep anesthesia. Extracted teeth were then replanted into the original cavity to allow the natural repair of the PDL. The replanted teeth were collected at 3, 7, and 14 days after transplantation and subjected to immunohistochemical analysis using the Kawamoto tape method or *in situ* hybridization as described in the supplemental Methods.

Generation of Transgenic Bioengineered Tooth Germ—Molar tooth germs were dissected from the mandibles of E14.5 mice. The isolation of mesenchyme and epithelium and the dissociation of mesenchymal cells have been described previously (24). Dissociated cells were cultured on tissue culture plates in DMEM containing 10% fetal calf serum and then infected with Adamtsl6β adenovirus for 8 h. After incubation for 24 h, mesenchymal cells overexpressing Adamtsl6β were collected via trypsin digestion and precipitated by centrifugation in a siliconized tube, and the supernatant was completely removed. The cell density of the precipitated, adenovirus-infected mesenchymal cells after removal of supernatant reached a concentration of 5×10^8 cells/ml, as described previously (24). Transgenic bioengineered tooth germ was reconstituted with dissociated adenovirus-infected mesenchymal cells and epithelial tissue using our previously described three-dimensional cell manipulation system, the organ germ method (24). The transgenic bioengineered tooth germs were incubated for 10 min at 37 °C, placed on cell culture inserts (0.4-μm pore diameter; BD Biosciences), and then further incubated at 37 °C for 6 days in an *in vitro* organ culture as described previously (24). Mesenchymal cells infected with lentiviruses carrying *Adamtsl6β* miRNAi were used to generate *Adamtsl6β* miRNAi-transgenic bioengineered tooth germ by incubation for 10 min at 37 °C, placement on cell culture inserts (0.4-μm pore diameter; BD Biosciences), and then a further incubation at 37 °C for 12 days in an *in vitro* organ culture as described previously (24).

Local Administration of ADAMTSL6β Using a PDL Injury Model—To create gels for injection, 2 μl of recombinant Adamtsl6β (10 μg/μl) (see supplemental Methods) and 1.5 μl of PKH67 green fluorescent cell linker (Sigma-Aldrich) were suspended in a 9-μl gel drop of collagen liquid Cellmatrix type I-A (Nitta Gelatin) composed of acid-soluble collagen isolated from pig tendon. The lower first molars of 4-week-old C57BL/6(SLC) mice were extracted under deep anesthesia. Following blood coagulation, at 3 days after tooth extraction, the alveolar bony wall of the proximal site of the lower second molar tooth was surgically removed to expose the PDL. The PDL was then disrupted by dislocation of the second molar tooth with lingual to buccal side movement. The collagen drop containing recombinant Adamtsl6β was then inserted into the damaged PDL. Mouse mandibles were collected 17 days after insertion, and immunohistochemical analysis was performed using the Kawamoto tape method as described in the supplemental Methods.
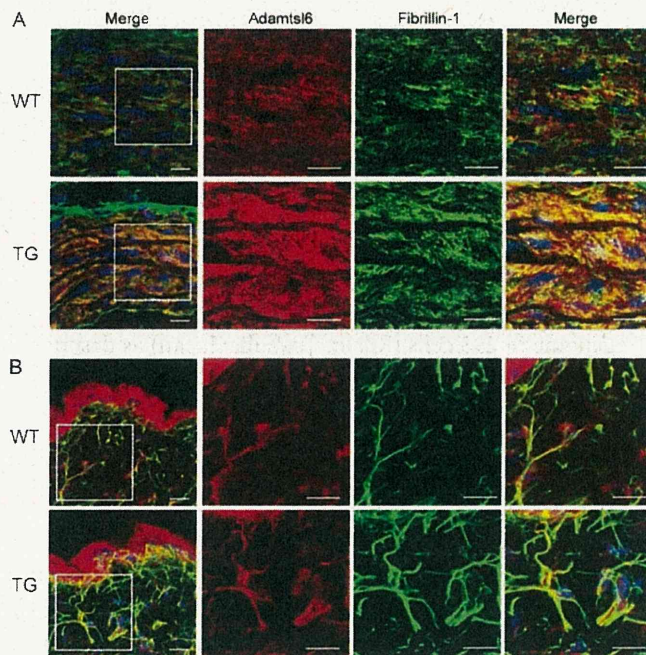

FIGURE 1. **Immunohistochemical analysis of *Tsl6β*-TG mice.** Immunofluorescence detection of ADAMTSL-6 proteins and fibrillin-1. Frontal cryosections were prepared from the skin (*A*) or aortas (*B*) of wild type (*top*) or *Tsl6β*-TG (*bottom*) littermates and subjected to double immunostaining with antibodies against Adamtsl6 (*red*) and fibrillin-1 (*green*). The *boxed areas* in the *leftmost panels* are shown at higher magnification in the *rightmost panels*. Immunohistochemical analysis indicated that the expression of Adamtsl6- and fibrillin-1-positive microfibrils was markedly increased in the aorta and skin of *Tsl6β TG* mice compared with WT mice. The *merged images* illustrate that these fibrils are colocalized in the skin and aorta.

RESULTS

ADAMTSL6β Regulates Microfibril Assembly in Various Connective Tissues—To investigate whether *Adamtsl6β* plays a critical role in microfibril assembly in connective tissues, we generated *Adamtsl6β*-transgenic mice (*Tsl6β*-TG mice) in which the transgene is expressed in the whole body. Because Adamtsl6 has been shown to be expressed in the aorta and skin, we investigated microfibril assembly of these tissues in the *Tsl6β*-TG mice. Immunohistochemical analysis revealed that Adamtsl6-positive microfibril assembly was barely detectable in WT mice but strongly induced in the aorta of *Tsl6β*-TG mice (Fig. 1*A*). Confocal microscopy analysis further revealed that Adamtsl6- and fibrillin-1-positive microfibrils are clearly increased in the aorta and that microfibril assembly is also induced in the skin of *Tsl6β*-TG mice. This confirmed that Adamtsl6 induces fibrillin-1 microfibril assembly in connective tissue, such as the aorta and skin (Fig. 1*B*).

ADAMTSL6β Is Involved in Microfibril Formation during PDL Development and Wound Healing—To investigate whether Adamtsl6β contributes to connective tissue formation, we first examined its expression patterns during embryonic tooth germ development and in the PDL formation stage after birth as a model of connective tissue formation. Development of the PDL proceeds as follows: 1) the dental follicle (DF), the origin of the PDL, is formed at the CAP stage of tooth germ formation; 2) the DF differentiates during the tooth root-forming stage; and 3) the DF differentiates into the PDL to be
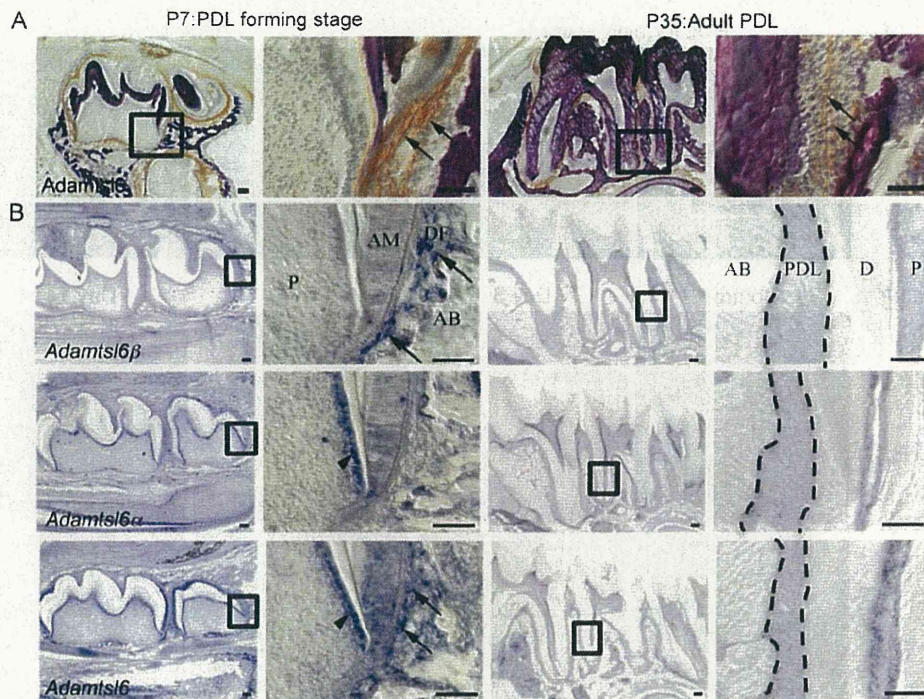
FIGURE 2. **Expression patterning of Adamtsl6α and -β during the PDL-forming stage.** *A,* sagittal sections of lower molar at P7 and P35 were immunostained with anti-Adamtsl6 antibody. The *image* in the *box* on the *left* is shown at higher magnification on the *right*. Note that Adamtsl6 protein was deposited as microfibril aggregates in DF at the PDL-forming stage (*arrows*) and formed a mature microfibrillar assembly in adult PDL (*arrows*). Bar, 100 μm. *B, in situ* hybridization analysis using a specific probe for *Adamtsl6α* and *-β* and control probe are shown. *Adamtsl6β* mRNA at the P1-late bell stage of dental follicle formation in the tooth germ is indicated by *arrows*. Expression of *Adamtsl6α* was detected in the odontoblast (*arrowheads*) by specific probes. In contrast, control probes that detected the conserved region of Adamtsl6 recognized both odontoblast (*arrowhead*) and DF (*arrows*). Bar, 100 μm. *AB,* alveolar bone; *AM,* ameloblast; *D,* dentin; *P,* pulp; *DF,* dental follicle; *PDL,* periodontal ligament.

inserted into collagen fibers known as Sharpey's fibers in the cementum matrix and alveolar bone, which resembles tendinous tissue (26, 31). *In situ* hybridization analysis revealed that *Adamtsl6β* is barely expressed in the DF, the origin of PDL formation in the surrounding tooth germ (supplemental Fig. S1*B*), but was very strongly expressed in the PDL-forming stage of the DF at P7 (Fig. 2*B*). However, *Adamtsl6β* expression was significantly down-regulated in the adult PDL at P35 (Fig. 2*B*). In contrast to *Adamtsl6β*, *Adamtsl6α* was found to be expressed in odontoblasts but not to be expressed in either the DF during the PDL-forming stage or in the adult PDL (supplemental Fig. S1*B* and Fig. 2*B*). Immunohistochemical analysis further revealed that Adamtsl6 is only weakly expressed in the early stage (bell stage) DF (supplemental Fig. S1*A*) but became detectable in assembled microfibril-like structures during the PDL-forming stage of the DF and in organized microfibrils in the adult PDL (Fig. 2*A*). Using confocal microscopy analysis, Adamtsl6 was observed to colocalize with fibrillin-1 to form immature microfibrillar-like structures at the PDL-forming stage of the DF, which were then observed as fully assembled mature microfibril structures in the adult PDL (Fig. 3*A*).

Using an Adamtsl6 antibody, positively stained fibers were observed in the adult PDL that were almost identical to those marked by aldehyde fuchsin staining and are indicative of microfibrils (supplemental Fig. S2). This suggested that Adamtsl6 was a component of microfibrils. Because developmental processes involve similar mechanisms to wound healing, we next determined whether Adamtsl6β is involved in PDL

microfibril assembly during wound healing using a tooth replantation model (supplemental Fig. S3*A*) (30). Histochemical analysis revealed an injured PDL with an irregular architecture at 3 days after replantation, although gradual healing then occurred at between 7 and 14 days after replantation (Fig. 3*B* and supplemental Fig. S3*B*). During these processes, *Adamtsl6β* and fibrillin-1 mRNA expression were found to be clearly induced in the PDL at 3–7 days after replantation but to decrease again by 14 days after replantation (Fig. 3*B*).

Similar to these gene expression patterns, Adamtsl6- and fibrillin-1-positive microfibrillar-like structures resembling those seen in the DF during the PDL-forming stage were markedly increased in the damaged PDL at 3–7 days after replantation. These structures had evolved into mature microfibrils by 14 days after replantation (Fig. 3*C* and supplemental Fig. S3*B*). In contrast to these gene expression patterns, the expression of periostin, a PDL differentiation marker, was detected at 7 days after replantation (supplemental Fig. S3*C*). These data indicate that fibrillin-1 microfibril formation is induced in the early stages of both PDL development and wound healing and that Adamtsl6β is involved in these processes.

ADAMTSL6β Regulates PDL Formation through Fibrillin-1 Microfibril Assembly—We have recently developed a new three-dimensional single cell processing technique, the organ germ method, which can be used to generate bioengineered tooth germ reconstituted from E14.5 molar tooth germ-derived epithelial and mesenchymal cells (24). Utilizing this system, we developed a transgenic bioengineered tooth germ by overex-
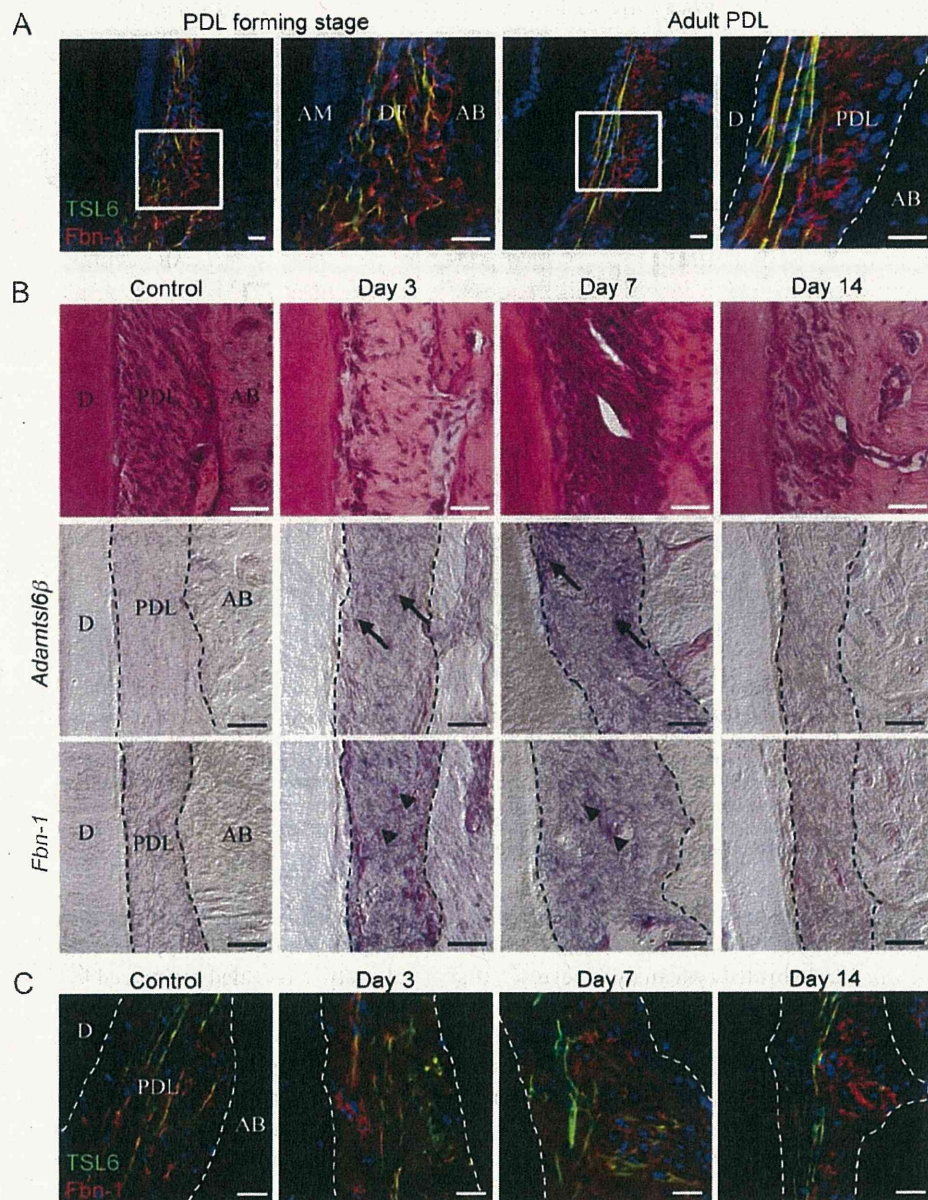
FIGURE 3. **Adamtsl6β is involved in fibrillin-1 microfibril formation during PDL development and wound healing.** *A*, localization of fibrillin-1- and Adamtsl6-positive microfibrils were analyzed during the PDL formation stage (*left*) and in adult PDL (*right*) using antibodies against Adamtsl6 (*TSL6; green*) and fibrillin-1 (*Fbn-1; red*). Formation of microfibrils positive for anti-Adamtsl6β and anti-fibrillin-1 was detectable during the process of PDL formation. *B*, frontal section of control side PDL and injured PDL 3, 7, and 14 days after replantation of the tooth were analyzed by hematoxylin and eosin staining (*top*) and *in situ* hybridization analysis of Adamtsl6β (*middle*) or fibrillin-1 (*Fbn-1; bottom*) expression in PDL. Cells positive for Adamtsl6β and fibrillin-1 mRNA expression are indicated by *arrows* or *arrowheads*, respectively. *C*, immunohistochemical analysis using anti-Adamtsl6 (*TSL6; green*) and anti-fibrillin-1 (*Fbn-1; red*) antibodies indicated that expression of Adamtsl6- and fibrillin-1-positive microfibrils was markedly increased 3 and 7 days after injury. A *merged image* illustrates that these fibrils were colocalized during the wound healing processes.

pressing exogenous genes in mesenchymal cells derived from tooth germ using adenovirus (supplemental Fig. S4, *A* and *B*). Because transgenic bioengineered tooth germ was found to accurately reproduce PDL development (supplemental Fig. S4, *C* and *D*), we generated *Adamtsl6β*-transgenic bioengineered tooth germ to examine the contributions of Adamtsl6β to PDL formation. Following immunohistochemical staining, *Adamtsl6β*-transgenic bioengineered tooth germs showed clear colocalization between fibrillin-1 microfibrils and Adamtsl6β (Fig. 4*A*) after 6 days of culture. Conversely, fibril-

lin-1 microfibrils were barely detectable in control *LacZ*-transgenic bioengineered tooth germ (Fig. 4*A*).

To confirm the role of Adamtsl6β in regulating microfibril formation in the DF from bioengineered tooth germ, we generated *Adamtsl6β* miRNAi-transgenic bioengineered tooth germ to suppress *Adamtsl6β* expression. Immunohistochemical analysis subsequently revealed that the *Adamtsl6β* miRNAi-transgenic germ exhibited poor Adamtsl6- and fibrillin-1-positive microfibril formation after 12 days of culture. However, no changes were observed in control miRNAi-transgenic bioengi-
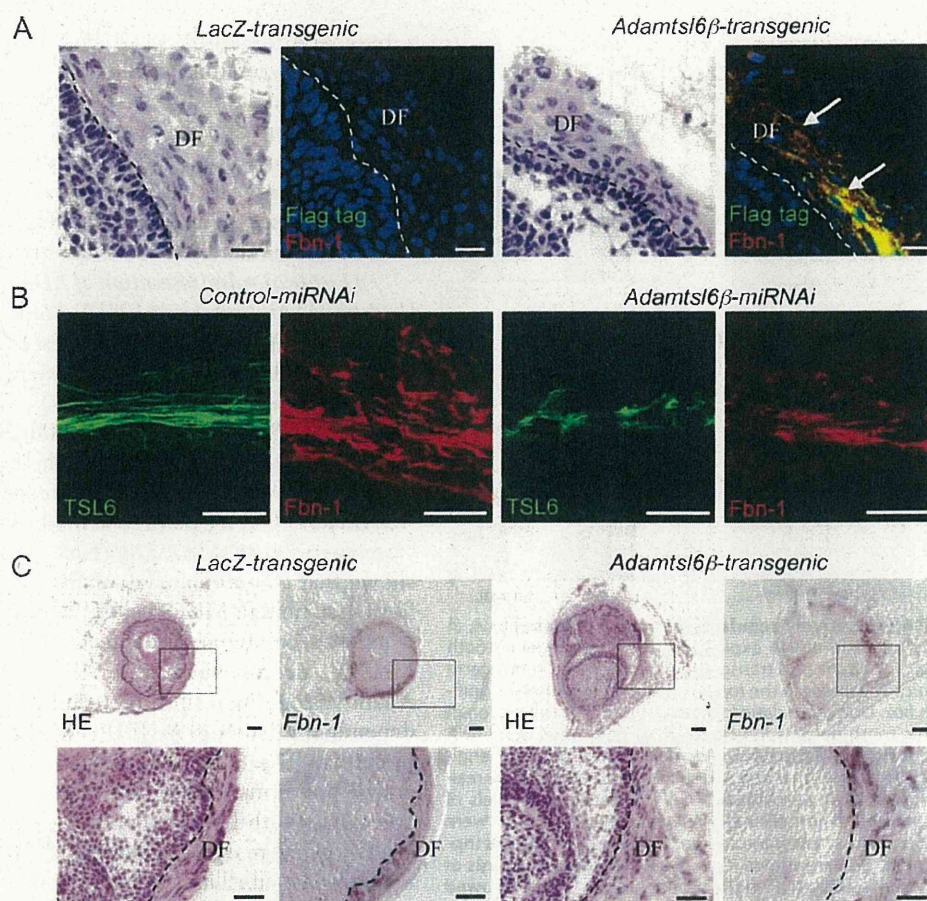
FIGURE 4. **Adamtsl6β contributes to PDL formation through regulation of fibrillin-1 microfibril assembly.** *A*, immunohistochemical analysis of *LacZ*-transgenic tooth germ (*LacZ-transgenic*) or *Adamtsl6β*-transgenic bioengineered tooth germ (*Adamtsl6β-transgenic*) using double immunostaining with anti-FLAG (*Flag tag*; *green*) and anti-fibrillin-1 (*Fbn-1*; *red*). Microfibrils positive for Adamtsl6β and fibrillin-1 expression are indicated by *arrows*. *B*, immunohistochemical analysis of control miRNAi-transgenic bioengineered tooth germ (*Control miRNAi*) or *Adamtsl6β* miRNAi-transgenic tooth germ (*Adamtsl6β-miRNAi*) using double immunostaining with anti-Adamtsl6 (*TSL6*; *green*) and anti-fibrillin-1 (*Fbn-1*; *red*). *C*, hematoxylin and eosin staining (*HE*) and *in situ* hybridization analysis of fibrillin-1 mRNA expression (*Fbn-1*) in *LacZ* transgenic tooth germ (*LacZ-transgenic*) or *Adamtsl6β* transgenic bioengineered tooth germ (*Adamtsl6β-transgenic*). The *image* in the *box* at the *top* is shown at higher magnification at the *bottom* (*C*).

neered tooth germ, further indicating that Adamtsl6β regulates microfibril assembly during PDL formation (Fig. 4*B*). We next evaluated whether the promotion of fibrillin-1 microfibril assembly was the result of increased mRNA expression. *In situ* hybridization analysis revealed that fibrillin-1 mRNA expression was similar in *LacZ*- and *Adamtsl6β*-transgenic bioengineered tooth germ (Fig. 4*C*). These data indicate that Adamtsl6β is capable of recruiting fibrillin-1 to assembling microfibrils without increasing the fibrillin-1 transcript levels.

ADAMTSL6β Negatively Regulates TGF-β-induced Periostin Gene Expression during PDL Formation—To investigate whether Adamtsl6β regulates PDL formation, we analyzed the expression of genes that function in PDL formation, including type I collagen, type XII collagen, periostin, and f-spondin (27). Among these genes, periostin, the protein product of which is known to be induced by TGF-β (32, 33), was markedly down-regulated in *Adamtsl6β*-transgenic bioengineered tooth germ (Fig. 5*B* and supplemental Fig. S5). *In situ* hybridization analysis further revealed the strong expression of periostin in the DF from *LacZ*-transgenic tooth germ when compared with the DF from *Adamtsl6β*-transgenic tooth germ (Fig. 5*A*). Real-time

PCR analysis confirmed the suppression of periostin expression in *Adamtsl6β*-transgenic tooth germ (Fig. 5*B*).

To evaluate whether Adamtsl6β negatively regulates periostin gene expression in our MFS model system, we analyzed *Adamtsl6β* adenovirus-infected tooth germ obtained in MFS mice that were homozygous for a targeted hypomorphic allele (mgR/mgR) of fibrillin-1 (7). *In situ* hybridization analysis showed that periostin expression was remarkably reduced in developing tooth germ from mgR/mgR mice after infection with *Adamtsl6β*-adenovirus compared with *LacZ*-adenovirus-infected tooth germ (Fig. 5*C*). We next investigated the effects of ADAMTSL6β on human PDL cells obtained from an MFS patient with severe periodontitis (MHPDL) (25). As expected, *ADAMTSL6β* overexpression in these MHPDL cells clearly reduced periostin expression when compared with mock-infected cells. Interestingly, the level of periostin expression in MHPDL cells with *ADAMTSL6β* overexpression was comparable with that of normal HPDL cells (Fig. 5*D*), raising the possibility that ADAMTSL6β negatively regulates TGF-β and thereby reduces periostin expression. We evaluated this possibility by testing the ability of His-tagged recombinant Adamtsl6β to bind to TGF-β1. Interactions between
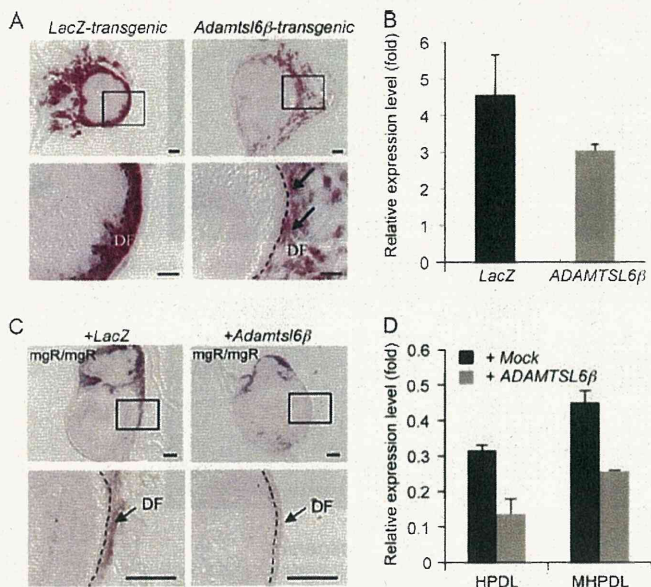
FIGURE 5. **ADAMTSL6β negatively regulates periostin expression.** *A, in situ* hybridization for periostin mRNA expression in *LacZ* transgenic tooth germ (*LacZ-transgenic*) or *Adamtsl6β* transgenic bioengineered tooth germ (*Adamtsl6β-transgenic*). The *image* in the *top box* is shown at higher magnification in the *bottom box*. Down-regulation of periostin mRNA expression in *Adamtsl6β* transgenic tooth germ is indicated by the *arrows*. *B*, total RNA extracted from *LacZ* (*LacZ*)- or *Adamtsl6β* (*Adamtsl6β*)-transgenic bioengineered tooth germ. cDNA was synthesized and subjected to quantitative real-time PCR for the expression of periostin and *GAPDH* transcripts. Levels of *GAPDH* transcript were used to normalize cDNA levels. Levels of *GAPDH* were set at 1, and relative expression levels are shown. Data are presented as triplicates, and the means ± S.D. are shown. *C, in situ* hybridization analysis of *Adamtsl6β*-adenovirus-infected mgR/mgR mouse tooth germ showed reduced periostin expression when compared with *LacZ*-adenovirus-infected mgR/mgR mouse tooth germ. *Bar*, 100 μm. *D*, real-time PCR analysis of periostin mRNA in HDPL and MHPDL cells transduced with mock or *Adamtsl6β*. Periostin mRNA expression was down-regulated in HPDL and MHPDL cells overexpressing *Adamtsl6β* as compared with expression in mock-overexpressed HPDL and MHPDL cells.
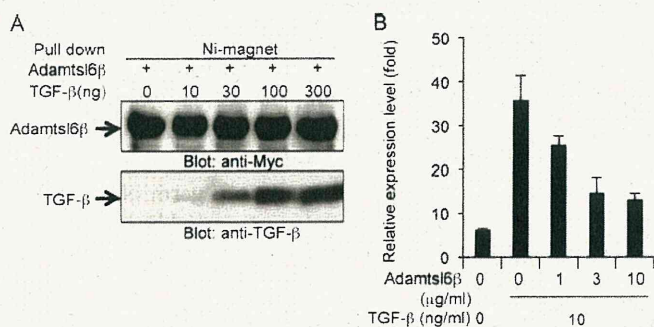

FIGURE 6. **Adamtsl6β binds TGF-β to negatively regulate periotsin gene expression.** *A*, His tag recombinant Adamtsl6β was incubated with TGF-β1 at the indicated concentrations followed by treatment with nickel-magnetic beads. Co-precipitates were detected using the corresponding antibodies, and Adamtsl6β was found to bind to TGF-β1 directly. *B*, mouse dental follicle cells were cultured with TGF-β1 for 3 days in the presence of recombinant mouse Adamtsl6β. Periostin mRNA levels were quantified by real-time PCR analysis. Adamtsl6β inhibited expression of periostin in a dose-dependent manner. *Error bars*, S.D.

Adamtsl6β and TGFβ1 were barely detectable at the 10 ng/ml concentrations, but strong associations between these proteins could be detected in a dose-dependent manner at 30, 100, or 300 ng/ml by pull-down analysis using nickel-magnetic beads (Fig. 6*A*). To then test the effects of recom-

binant Adamtsl6β on TGF-β activity, we measured the periostin expression levels in mouse dental follicle cells treated with Adamtsl6β in the presence or absence of TGF-β1. Recombinant Adamtsl6β inhibited TGF-β-induced periostin expression in a dose-dependent manner (Fig. 6*B*). These data suggest that Adamtsl6β directly binds to TGF-β to reduce periostin expression during the PDL-forming stage in both normal and MFS model settings.

The Local Administration of ADAMTSL6β Improves Wound Healing Ability in an MFS Model—We next investigated whether ADAMTSL6β alleviates fibrillin-1 microfibril disorder in MHPDL cells, which exhibit reduction in fibrillin-1 microfibril assembly (Fig. 7). The overexpression of *ADAMTSL6β* strongly induced fibrillin-1 microfibril assembly in MHPDL cells compared with the mock-infected controls (Fig. 7, *top* and *middle*). *Merged images* revealed that ADAMTSL6β colocalizes with fibrillin-1 in MHPDL cells that overexpress *ADAMTSL6β* (Fig. 7, *bottom*). We have previously shown that recombinant Adamtsl6β induces fibrillin-1 microfibril assembly in MG63 cells (17). Thus, we next investigated whether recombinant Adamtsl6β improves the symptoms of MHPDL microfibril disorder. We found that recombinant Adamtsl6β induces fibrillin-1 microfibril assembly in a dose-dependent manner in MHPDL cells during a 3-day incubation in culture (Fig. 8, *top* and *middle*). Staining with an anti-Adamtsl6 polyclonal antibody indicated that exogenous Adamtsl6 colocalizes with fibrillin-1 (Fig. 8, *bottom*). Endogenous fibrillin-1 was only marginally detectable in MHPDL cells. However, an abundant fibrillin-1 network formation was evident in the presence of high concentrations (10 μg/ml) of recombinant Adamtsl6β (Fig. 8, *top*). These results indicate that Adamtsl6β improved fibrillin-1 MHPDL microfibril assembly.

To investigate whether Adamtsl6β was capable of improving microfibril assembly *in vivo*, we investigated the PDL from mgR/mgR mice and by histochemical analysis observed a disorganized structure with a disrupted cell alignment, both of which are characteristic MFS morphologies (Fig. 9*A*). Immunohistochemical analysis clearly revealed fragmented Adamtsl6β- and fibrillin-1-positive microfibrils when compared with wild type mice (Fig. 9*A, arrows*). We next infected *Adamtsl6β* adenovirus into the DF of developing tooth germ isolated from mgR/mgR mouse embryos at E14.5 to evaluate the improvements in fibrillin-1 microfibril disorder during PDL formation. By histochemical analysis, we found that the overexpression of *Adamtsl6β* resulted in an improved DF morphology with compact and aligned cells (Fig. 9*B*). DF tooth germ infected with *LacZ* showed low cell numbers and an irregular architecture. Immunohistochemical analysis subsequently revealed that *Adamtsl6β* overexpression strongly induces fibrillin-1 microfibril assembly in the tooth germ from mgR/mgR mice, whereas no assembly was observed in *LacZ*-infected tooth germ (Fig. 9*B, arrows*). These data indicate that Adamtsl6β can indeed restore the impaired microfibrils in mgR/mgR mice.

We next investigated whether Adamtsl6β might be developed as a novel therapeutic for MFS microfibril disorder. Collagen gel containing recombinant Adamtsl6β was locally administrated into an experimentally damaged PDL in mgR/
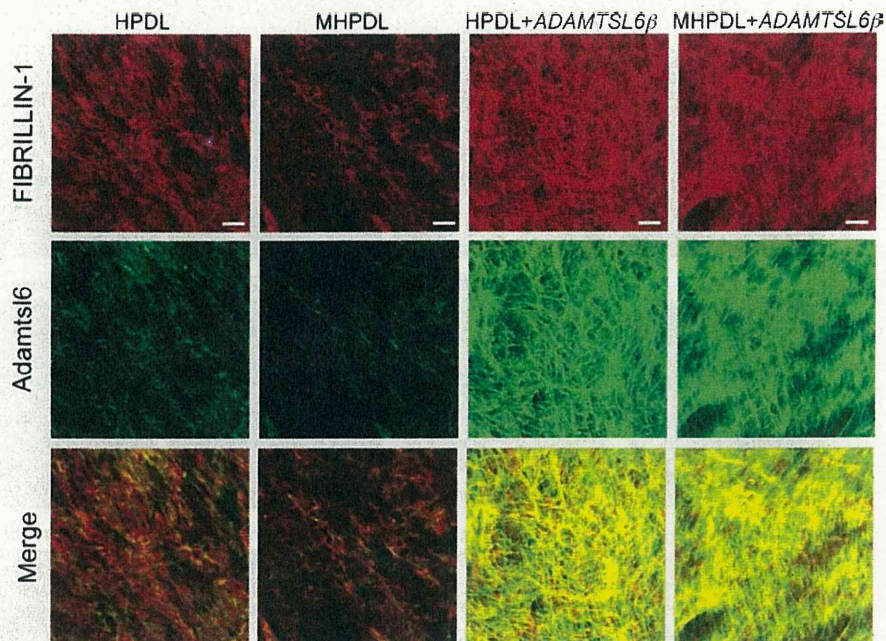
FIGURE 7. Overexpression of *ADAMTSL6β* improves microfibril disorder in PDL from an MFS patient. Immunohistochemical analysis of HPDL or MHPDL cells transduced with mock or *ADAMTSL6β* using anti-fibrillin-1 (*top*) and anti-ADAMTSL6 (*middle*) antibodies. The data show that ADAMTSL6β induces fibrillin-1 microfibril assembly in MHPDL cells. The *bottom images* were produced by superimposition of the *upper* and *middle images,* together with DAPI nuclear staining.
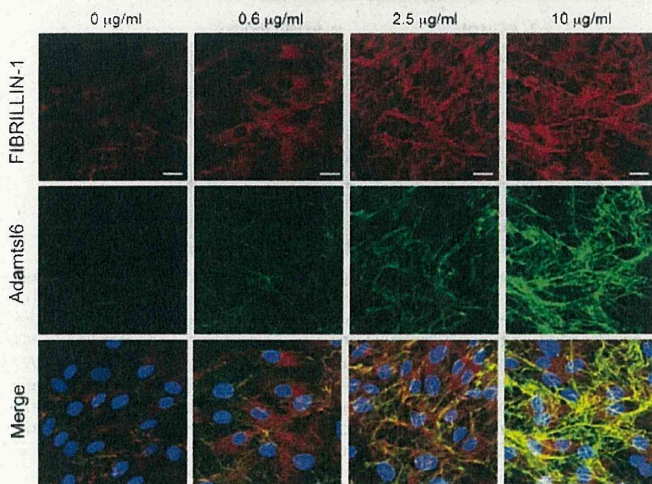

FIGURE 8. Recombinant Adamtsl6β improves microfibril disorder in PDL from MFS patients. Immunohistochemical analysis with anti-fibrillin-1 (*top*) and anti-Adamtsl6 (*middle*) antibodies reveals a marked improvement in fibrillin-1 microfibril assembly (*arrows*) in MHPDL cells incubated with purified recombinant Adamtsl6β at 0.6, 2.5, and 10 μg/ml for 3 days. The *bottom images* were produced by superimposition of the *upper* and *middle images,* together with DAPI nuclear staining.

mgR mice (supplemental Fig. S6, *A* and *B*). Fluorescence microscopic analysis revealed that the collagen gel implanted in damaged PDL was still present at 17 days after injection (supplemental Fig. S6C). Histochemical analysis showed that a damaged PDL could still be observed at 7 days after injection of the collagen gel containing recombinant Adamtsl6β (supplemental Fig. S6D). However, healing and improved cell alignment were apparent in the PDL of wild type mice at 17 days after injection (Fig. 9C, *asterisk*). Immunohistochemical analysis further revealed that the reorganization of fibril-lin-1- and Adamtsl6-positive microfibril assembly could be observed after 17 days of incubation (Fig. 9C (*arrowheads*) and supplemental Fig. S6E). In contrast, the administration of control collagen gel failed to induce PDL healing, and an irregular cell morphology and poor fibrillin-1 microfibril formation could still be observed (Fig. 9C and supplemental Fig. S6E).

The enhanced activation of TGF-β has been suggested to directly contribute to tissue destruction in MFS (12). Ligand-activated TGF-β receptors induce the phosphorylation of Smad2 and Smad3 (pSmad2/3), which form a heteromeric complex with Smad4 that translocates to the nucleus and mediates the expression of target genes (34). The nuclear accumulation of pSmad2/3 has been detected in affected tissues in an MFS mouse model, including the aorta and skeletal muscle (10, 35). Consistent with these results, we observed the nuclear accumulation of pSmad2/3 in PDL from mgR/mgR mice 17 days after injection of control collagen gel in our current experiments (Fig. 9D). However, the local administration of Adamtsl6β markedly suppressed the nuclear localization of pSmad2/3. Further evidence for the Adamtsl6β suppression of TGF-β signaling is derived from the previous analysis of matrix metalloprotease (MMP)-9, which is known to be induced by TGF-β and is expressed in abnormal smooth muscle cells in the early vascular lesions that contribute to elastolysis (36, 37). In contrast to control collagen gel administration, the expression of MMP-9 was markedly suppressed by the administration of collagen gel containing recombinant Adamtsl6β (Fig. 9D). These results illustrate that reorganization of microfibrils by recombinant Adamtsl6β prevents the pathological activation of TGF-β by structurally damaged fibrillin-1 in MFS.
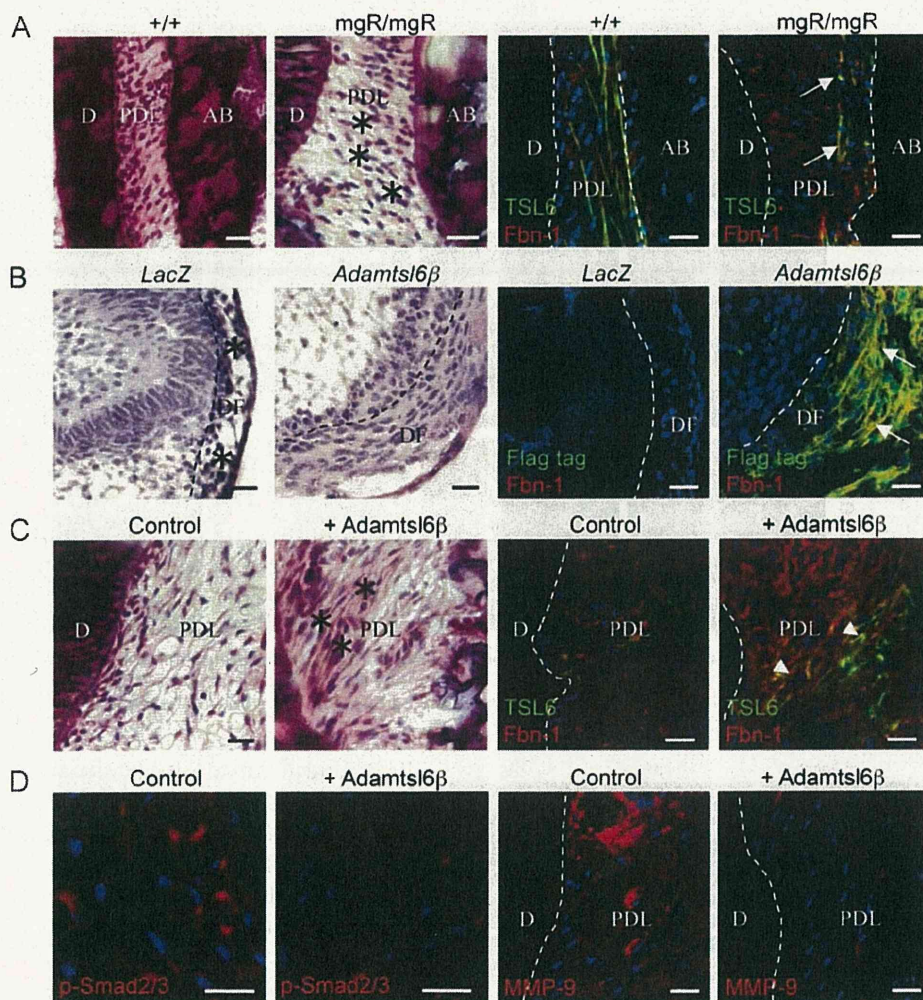
FIGURE 9. **Local administration of Adamtsl6β improves microfibril disorder and attenuates TGF-β signaling in PDL from an MFS model.** *A*, hematoxylin and eosin staining of a PDL revealing a markedly abnormal architecture in mgR/mgR mice when compared with wild type. Notable is the loosening of the PDL with an irregular cell alignment and an expanded cell-cell distance (*asterisks*). Immunohistochemical analysis using Adamtsl6 (*TSL6; green*) and fibrillin-1 (*Fbn-1; red*) antibodies revealed a clear disruption of fibrillin-1- and Adamtsl6-positive microfibrils in the PDL from mgR/mgR mice (*arrows*). *B*, hematoxylin and eosin staining of *LacZ*-infected mgR/mgR mouse tooth germ (*LacZ*) revealing an abnormal architecture with an irregular cell alignment (*asterisks*) when compared with *Adamtsl6β*-infected mgR/mgR mouse tooth germ (*Adamtsl6β*). Immunohistochemical analysis using FLAG (*Flag-tag; green*) and fibrillin-1 (*Fbn-1; red*) antibodies showed an improvement in fibrillin-1 microfibril assembly in *Adamtsl6β*-infected mgR/mgR mouse tooth germ (*arrows*). *C*, histological analysis of the injured PDL in mgR/mgR mice after the local administration of control gel or gel containing recombinant Adamtsl6β for 17 days. Hematoxylin and eosin staining revealed PDL healing after the injection of gel containing recombinant Adamtsl6β (*asterisks*) compared with the control. Immunohistochemical analysis further showed an improvement in fibrillin-1 microfibril assembly (*arrowheads*) induced by the injection of recombinant Adamtsl6β. *D*, immunohistochemical analysis of pSmad2/3 and MMP-9 expression in the injured PDL of mgR/mgR mice after the local administration of control gel or gel containing recombinant Adamtsl6β for 17 days. The suppression of nuclear accumulation of pSmad2/3 and MMP-9 expression is evident after injection of recombinant Adamtsl6β compared with the control gel.

DISCUSSION

Our current experiments successfully demonstrate that ADAMTSL6β has an essential role in PDL development and regeneration through the promotion of fibrillin-1 assembly and the negative regulation of TGF-β signaling. We also demonstrate in our present analyses that the local administration of ADAMTSL6β can rescue the disease manifestations of MFS in a mouse model, raising the possibility that this extracellular matrix protein could be used as a novel therapeutic agent for the treatment of MFS. Hence, our data show for the first time that the restoration of properly formed microfibrils by ADAMTSL6β is essential not only for improvement of the predominant symptoms of MFS but also for the suppression of excessive TGF-β signaling induced by microfibril disassembly.

To clarify the role of ADAMTSL6β in PDL formation, experiments were performed to determine whether ADAMTSL6β-mediated fibrillin-1 microfibril assembly is critical for PDL development and regeneration. The formation of fibrillin-1 microfibril networks has been shown to be essential for the development and growth of individual organ systems (38). Vascular smooth muscle cells are gradually organized via the formation of elastic fibers and interconnecting fibrillin-1 microfibrils during aortic media generation, resulting in the organization of elastic lamellae as the main determinant of arterial function (39). In addition to providing mechanical stability, previous studies have demonstrated that the organization of fibrillin-1 microfibril assemblies contributes to the regulation of the activities of signaling molecules, such as TGF-β and

BMP-7 (40, 41). During digit formation, fibrillin-1 may be a positive regulator that dictates the functional sites for cytokine concentration. In other tissues, fibrillin-1 acts as a negative regulator of signaling through cytokine sequestration (2, 7). Thus, the importance of microfibril network formation has been demonstrated in several disparate settings. However, the importance of the molecular mechanisms governing fibrillin-1 assembly during organogenesis has been hampered by the unanswered issue of the actual factor that drives microfibril assembly. Our present study demonstrates that ADAMTSL6β, an inducing factor for microfibril assembly (18), regulates development and regeneration of PDL. Furthermore, ADAMTSL6β-mediated fibrillin-1 microfibril assembly may accelerate the sequestration of large latent complexes of TGF-β or active TGF-β, thereby negatively regulating the expression of TGF-β regulatory targets, such as periostin (35, 42). Hence, our data provide significant insight into the molecular mechanisms by which ADAMTSL6β controls fibrillin-1 microfibril assembly and TGF-β signaling during organogenesis.

The establishment of fibrillin-1 microfibril assembly mechanisms is ultimately critical for the development of new MFS therapeutic approaches (12). The pathogenetic relevance of MFS is highlighted by the fact that microfibril assembly is frequently disrupted in patients with various fibrillinopathies (43). MFS fibrillinopathies have been explained by the structural insufficiency of fibrillin-1 microfibrils, leading to activation of TGF-β and its regulatory targets (7, 44). Although many recent publications have addressed the organization of fibrillins in microfibrils (45–48), relatively little information has been available regarding the mechanisms and components involved in microfibril formation. A previous study reported that the transgenic expression of wild-type fibrillin-1 alleles in a missense mutation (C1039G) heterozygous mouse model of MFS effectively rescues the aortic phenotype (11). From these data, essential improvements in fibrillin-1 microfibril formation represent a productive therapeutic strategy for the reduction of MFS disease severity (3).

In contrast to our present findings, another recent study has indicated that fibronectin is an essential component in the assembly of fibrillin-1 through its interaction with the C-terminal region of fibrillin-1, thus suggesting the possibility of improved microfibril assembly through regulation of fibrillin-1-associated proteins (49, 50). Our present data demonstrate, however, that the exogenous application of recombinant ADAMTSL6β improves fibrillin-1 microfibril assembly in an MFS mouse model. Hence, ADAMTSL6β reinforcement of fibrillin-1 microfibrils may represent a new, viable treatment for MFS. Although the mechanisms by which ADAMTSL6β accelerated fibrillin-1 microfibril assembly remain to be determined, in another study using the MFS mouse model and MHPDL cells, which are PDL cells obtained from an MFS patient, ADAMTSL6β seems to recruit available normal fibrillin-1 molecules and induce microfibril assembly with a resulting improvement in microfibril mechanical stability. These findings indicate that ADAMTSL6β is capable of enhancing microfibrils even in animals with a fibrillin-1 haploinsufficiency. Thus, ADAMTSL6β is potentially a novel therapeutic target for the treatment of MFS.

Recent evidence has suggested that restoration of microfibril assembly plays an important role in the prevention of pathological activation of TGF-β signaling in MFS (12). TGF-β is secreted from cells as a large latent complex consisting of TGF-β, latency-associated peptide, and LTBP-1 to be sequestered by fibrillin-1 (51). The promotion of fibrillin-1 microfibril assembly is therefore critical for the prevention of tissue destruction mediated by abnormal TGF-β signaling in MFS. In the present study, we have demonstrated that the reinforcement of fibrillin-1 microfibril assembly and the inhibition of TGFβ1 function by ADAMTSL6β facilitate wound healing in the PDL of mgR/mgR mice.

In conclusion, we provide evidence for the contributions of ADAMTSL6β-mediated fibrillin-1 microfibril assembly to PDL development, regeneration, and alleviation of MFS manifestations. We thereby introduce the concept that a fibrillin-1-associated protein, such as ADAMTSL6β, which induces microfibril assembly, should be considered in the development of future mechanism-based therapeutics for the improvement of connective tissue disorders, such as MFS. Our data suggest that the reinforcement of fibrillin-1 assembly by ADAMTSL6β accelerates the sequestration of newly synthesized large latent complexes into fibrillin-1. Further studies will help to clarify the nature of the interactions between ADAMTSL6β, fibrillin-1, TGF-β, and LTBP-1 and reveal how ADAMTSL6β expression suppresses TGF-β signaling. It will also be necessary to develop methodologies for the systemic administration of ADAMTSL6β to induce fibrillin-1 microfibril assembly in connective tissue for the treatment of life-threatening conditions, such as aortic aneurysm. Because elastolysis occurs continuously in aortic aneurysms in MFS, chronic administration of ADAMTSL6β may be required for the stabilization of microfibrils to prevent progressive tissue destruction. This approach will facilitate drug discovery for treating MFS and related connective tissue disorders.

REFERENCES

1. Straub, A. M., Grahame, R., Scully, C., and Tonetti, M. S. (2002) *J. Periodontol.* **73,** 823–826
2. Ramirez, F., and Dietz, H. C. (2007) *J. Cell Physiol.* **213,** 326–330
3. Judge, D. P., and Dietz, H. C. (2005) *Lancet* **366,** 1965–1976
4. Dietz, H. C., Loeys, B., Carta, L., and Ramirez, F. (2005) *Am. J. Med. Genet. C Semin. Med. Genet.* **139,** 4–9
5. Sakai, L. Y., Keene, D. R., and Engvall, E. (1986) *J. Cell Biol.* **103,** 2499–2509
6. Ramirez, F., and Dietz, H. C. (2007) *Curr. Opin. Genet. Dev.* **17,** 252–258
7. Pereira, L., Lee, S. Y., Gayraud, B., Andrikopoulos, K., Shapiro, S. D., Bunton, T., Biery, N. J., Dietz, H. C., Sakai, L. Y., and Ramirez, F. (1999) *Proc. Natl. Acad. Sci. U.S.A.* **96,** 3819–3823
8. Neptune, E. R., Frischmeyer, P. A., Arking, D. E., Myers, L., Bunton, T. E., Gayraud, B., Ramirez, F., Sakai, L. Y., and Dietz, H. C. (2003) *Nat. Genet.* **33,** 407–411
9. Carta, L., Pereira, L., Arteaga-Solis, E., Lee-Arteaga, S. Y., Lenart, B.,

Starcher, B., Merkel, C. A., Sukoyan, M., Kerkis, A., Hazeki, N., Keene, D. R., Sakai, L. Y., and Ramirez, F. (2006) *J. Biol. Chem.* **281,** 8016–8023

10. Habashi, J. P., Judge, D. P., Holm, T. M., Cohn, R. D., Loeys, B. L., Cooper, T. K., Myers, L., Klein, E. C., Liu, G., Calvi, C., Podowski, M., Neptune, E. R., Halushka, M. K., Bedja, D., Gabrielson, K., Rifkin, D. B., Carta, L., Ramirez, F., Huso, D. L., and Dietz, H. C. (2006) *Science* **312,** 117–121

11. Judge, D. P., Biery, N. J., Keene, D. R., Geubtner, J., Myers, L., Huso, D. L., Sakai, L. Y., and Dietz, H. C. (2004) *J. Clin. Invest.* **114,** 172–181

12. Judge, D. P., and Dietz, H. C. (2008) *Annu. Rev. Med.* **59,** 43–59

13. Ng, C. M., Cheng, A., Myers, L. A., Martinez-Murillo, F., Jie, C., Bedja, D., Gabrielson, K. L., Hausladen, J. M., Mecham, R. P., Judge, D. P., and Dietz, H. C. (2004) *J. Clin. Invest.* **114,** 1586–1592

14. Hirohata, S., Wang, L. W., Miyagi, M., Yan, L., Seldin, M. F., Keene, D. R., Crabb, J. W., and Apte, S. S. (2002) *J. Biol. Chem.* **277,** 12182–12189

15. Le Goff, C., Morice-Picard, F., Dagoneau, N., Wang, L. W., Perrot, C., Crow, Y. J., Bauer, F., Flori, E., Prost-Squarcioni, C., Krakow, D., Ge, G., Greenspan, D. S., Bonnet, D., Le Merrer, M., Munnich, A., Apte, S. S., and Cormier-Daire, V. (2008) *Nat. Genet.* **40,** 1119–1123

16. Ahram, D., Sato, T. S., Kohilan, A., Tayeh, M., Chen, S., Leal, S., Al-Salem, M., and El-Shanti, H. (2009) *Am. J. Hum. Genet.* **84,** 274–278

17. Tsutsui, K., Manabe, R., Yamada, T., Nakano, I., Oguri, Y., Keene, D. R., Sengle, G., Sakai, L. Y., and Sekiguchi, K. (2010) *J. Biol. Chem.* **285,** 4870–4882

18. Sawada, T., Sugawara, Y., Asai, T., Aida, N., Yanagisawa, T., Ohta, K., and Inoue, S. (2006) *J. Histochem. Cytochem.* **54,** 1095–1103

19. Tsuruga, E., Irie, K., and Yajima, T. (2002) *J. Dent. Res.* **81,** 771–775

20. Staszyk, C., and Gasse, H. (2004) *Anat. Histol. Embryol.* **33,** 17–22

21. Kawamoto, T. (1990) *J. Histochem. Cytochem.* **38,** 1805–1814

22. Nishimura, R., Hata, K., Harris, S. E., Ikeda, F., and Yoneda, T. (2002) *Bone* **31,** 303–312

23. Yamamoto, T., Miyoshi, H., Yamamoto, N., Yamamoto, N., Inoue, J., and Tsunetsugu-Yokota, Y. (2006) *Blood* **108,** 3305–3312

24. Nakao, K., Morita, R., Saji, Y., Ishida, K., Tomita, Y., Ogawa, M., Saitoh, M., Tomooka, Y., and Tsuji, T. (2007) *Nat. Methods* **4,** 227–230

25. Shiga, M., Saito, M., Hattori, M., Torii, C., Kosaki, K., Kiyono, T., and Suda, N. (2008) *Cell Tissue Res.* **331,** 461–472

26. Handa, K., Saito, M., Yamauchi, M., Kiyono, T., Sato, S., Teranaka, T., and Sampath Narayanan, A. (2002) *Bone* **31,** 606–611

27. Nishida, E., Sasaki, T., Ishikawa, S. K., Kosaka, K., Aino, M., Noguchi, T., Teranaka, T., Shimizu, N., and Saito, M. (2007) *Gene* **404,** 70–79

28. Nakajima, M., Kizawa, H., Saitoh, M., Kou, I., Miyazono, K., and Ikegawa, S. (2007) *J. Biol. Chem.* **282,** 32185–32192

29. Yokoi, T., Saito, M., Kiyono, T., Iseki, S., Kosaka, K., Nishida, E., Tsubakimoto, T., Harada, H., Eto, K., Noguchi, T., and Teranaka, T. (2007) *Cell Tissue Res.* **327,** 301–311

30. Hasegawa, T., Suzuki, H., Yoshie, H., and Ohshima, H. (2007) *Cell Tissue Res.* **329,** 259–272

31. Nanci, A., and Bosshardt, D. D. (2006) *Periodontol 2000* **40,** 11–28

32. Goetsch, S. C., Hawke, T. J., Gallardo, T. D., Richardson, J. A., and Garry, D. J. (2003) *Physiol. Genomics* **14,** 261–271

33. Cheng, J., and Grande, J. P. (2002) *Exp. Biol. Med.* **227,** 943–956

34. Heldin, C. H., Miyazono, K., and ten Dijke, P. (1997) *Nature* **390,** 465–471

35. Cohn, R. D., van Erp, C., Habashi, J. P., Soleimani, A. A., Klein, E. C., Lisi, M. T., Gamradt, M., ap Rhys, C. M., Holm, T. M., Loeys, B. L., Ramirez, F., Judge, D. P., Ward, C. W., and Dietz, H. C. (2007) *Nat. Med.* **13,** 204–210

36. Chou, Y. T., Wang, H., Chen, Y., Danielpour, D., and Yang, Y. C. (2006) *Oncogene* **25,** 5547–5560

37. Bunton, T. E., Biery, N. J., Myers, L., Gayraud, B., Ramirez, F., and Dietz, H. C. (2001) *Circ. Res.* **88,** 37–43

38. Charbonneau, N. L., Ono, R. N., Corson, G. M., Keene, D. R., and Sakai, L. Y. (2004) *Birth Defects Res. C Embryo Today* **72,** 37–50

39. Brooke, B. S., Karnik, S. K., and Li, D. Y. (2003) *Trends Cell Biol.* **13,** 51–56

40. Gregory, K. E., Ono, R. N., Charbonneau, N. L., Kuo, C. L., Keene, D. R., Bächinger, H. P., and Sakai, L. Y. (2005) *J. Biol. Chem.* **280,** 27970–27980

41. Ramirez, F., and Rifkin, D. B. (2009) *Curr. Opin. Cell Biol.* **21,** 616–622

42. Massagué, J. (2008) *Mol. Cell* **29,** 149–150

43. Vollbrandt, T., Tiedemann, K., El-Hallous, E., Lin, G., Brinckmann, J., John, H., Bätge, B., Notbohm, H., and Reinhardt, D. P. (2004) *J. Biol. Chem.* **279,** 32924–32931

44. Hutchinson, S., Furger, A., Halliday, D., Judge, D. P., Jefferson, A., Dietz, H. C., Firth, H., and Handford, P. A. (2003) *Hum. Mol. Genet.* **12,** 2269–2276

45. Baldock, C., Siegler, V., Bax, D. V., Cain, S. A., Mellody, K. T., Marson, A., Haston, J. L., Berry, R., Wang, M. C., Grossmann, J. G., Roessle, M., Kielty, C. M., and Wess, T. J. (2006) *Proc. Natl. Acad. Sci. U.S.A.* **103,** 11922–11927

46. Lee, S. S., Knott, V., Jovanovi, J., Harlos, K., Grimes, J. M., Choulier, L., Mardon, H. J., Stuart, D. I., and Handford, P. A. (2004) *Structure* **12,** 717–729

47. Hubmacher, D., El-Hallous, E. I., Nelea, V., Kaartinen, M. T., Lee, E. R., and Reinhardt, D. P. (2008) *Proc. Natl. Acad. Sci. U.S.A.* **105,** 6548–6553

48. Kuo, C. L., Isogai, Z., Keene, D. R., Hazeki, N., Ono, R. N., Sengle, G., Bächinger, H. P., and Sakai, L. Y. (2007) *J. Biol. Chem.* **282,** 4007–4020

49. Sabatier, L., Chen, D., Fagotto-Kaufmann, C., Hubmacher, D., McKee, M. D., Annis, D. S., Mosher, D. F., and Reinhardt, D. P. (2009) *Mol. Biol. Cell* **20,** 846–858

50. Kinsey, R., Williamson, M. R., Chaudhry, S., Mellody, K. T., McGovern, A., Takahashi, S., Shuttleworth, C. A., and Kielty, C. M. (2008) *J. Cell Sci.* **121,** 2696–2704

51. Isogai, Z., Ono, R. N., Ushiro, S., Keene, D. R., Chen, Y., Mazzieri, R., Charbonneau, N. L., Reinhardt, D. P., Rifkin, D. B., and Sakai, L. Y. (2003) *J. Biol. Chem.* **278,** 2750–2757

Expert Opinion

Extracellular matrix administration as a potential therapeutic strategy for periodontal ligament regeneration

Masahiro Saito[†] & Takashi Tsuji

[†] Tokyo University of Science, Faculty of Industrial Science and Technology, Noda, Japan

Introduction: The current strategies employed for the treatment of connective tissue disease include the application of stem cells, the use of functional molecules that can reorganize tissue integrity and cellular activities to recover connective tissue function. Approaches to the regeneration of periodontal tissue, which is the tooth-supporting connective tissue, have made some progress recently and provide a useful experimental model for the evaluation of future strategies to treat connective tissue diseases such as periodontal disease.

Areas covered: The ultimate goal of periodontal tissue regeneration is to reconstruct the ligament structure that will sustain the required mechanical force to connect with mineralized tissues such as cementum and alveolar bone. In this review, we discuss the proposed use of extracellular matrix (ECM) administration therapy as an additional therapeutic strategy to stem cell transplantation and cytokine administration in the current field of periodontal tissue regeneration therapy.

Expert opinion: Although various available tissue engineering technologies can now achieve periodontal tissue regeneration, ECM administration therapy is likely to play an essential future role in the development and regeneration of periodontal tissue and attenuate the signaling events that mediate tissue degradation. Hence, ECM administration could serve as a novel technology in periodontal tissue regeneration and also as a viable approach to alleviating connective tissue disorders such as Marfan's syndrome.

1. Introduction

Periodontal tissue is a tooth-supporting tissue comprising periodontal ligament (PDL), cementum and alveolar bone. This tissue thereby plays an important role in the maintenance of the occlusion system. Among the components of periodontal tissue, the PDL consists mainly of an extracellular matrix (ECM) that provides the physical properties to withstand mechanical stress in cooperation with the cementum and alveolar bone. Dysfunction of the PDL occurs as a result of periodontal disease, an inflammatory disorder involving the irreversible destruction of periodontal tissues and requiring the regeneration of PDL as a treatment for recovering occlusion function [1,2]. Periodontal disease is caused by pathogenic microflora including *Porphyromonas gingivalis*, *Tannerella forsythia* and *Treponema denticola*, and the resulting inflammation extends deep into the periodontal tissue and causes the loss of PDL, cementum and alveolar bone [3]. Chronic periodontal disease is the most common form of this disorder, showing a prevalence rate of > 90% in adults

informa

healthcare

over 60 years of age [4]. Furthermore, this disorder is the major cause of tooth loss in adults of over 40 years and its more severe forms has a worldwide prevalence of up to 20% according to the World Health Organization [5]. Blocking the progression of periodontal disease has been achieved by mechanically removing bacterial biofilm with conventional periodontal and/or surgical treatments. These treatments can reduce the destruction of periodontal tissue and diminish inflammation in the affected region. However, achieving adequate periodontal tissue regeneration remains a problem, particularly in cases where the disease has caused large defects in the periodontal tissue.

The current advances in future regenerative therapies have been influenced by many previous studies of embryonic development, stem cell biology and tissue engineering technologies [6-9]. To restore the partial loss of organ functions and to repair damaged tissues, attractive concepts that have emerged in regenerative therapy is stem cell transplantation into various tissues and organs [10] and cytokine therapy, which has the potential to induce the activation and differentiation of tissue stem/progenitor cells [11]. Tooth tissue stem cells and the cytokine network that regulates tooth development, and dental tissue cell growth and differentiation, have been well characterized at the molecular level [12,13]. The regeneration of periodontal tissues is being made clinically possible by the transplantation of mesenchymal stem cells which can differentiate into PDL cells, cementoblasts and osteoblasts, or through the local application of cytokines to stimulate the proliferation and differentiation of these stem cells [14-17]. Although these therapies are effective and contribute to periodontal tissue repair, these interventions will likely be improved by an enhanced understanding of the

development of periodontal tissues, particularly those involved in the formation of PDL, cementum and alveolar bone.

The ECM is a biologically active molecule composed of a complex mixture of macromolecules that, in addition to serving a structural function, profoundly affect the cellular physiology of an organism [18]. Previous findings have revealed that ECM components including type I collagen, type III collagen, lumican, decorin, periostin, f-spondin, tenascin-N and PLAP1/aspirin are highly expressed during PDL formation [19,20]. Since the ECM is regulated in a tissue-specific manner, these structures could enhance periodontal regeneration by promoting the differentiation of cells required for the synthesis of PDL, bone and cementum [21,22]. Among the ECM formations in the PDL, fibrillin-1, a major component of the microfibrils that regulate tissue integrity and elasticity, has been shown to contribute to the formation and maintenance of this ligament. An abnormal PDL structure in association with the progressive destruction of microfibrils has been observed in a Marfan's syndrome (MFS) mouse model and has characteristics that are similar to those of fibrillin-1 dysfunction [23]. These findings have strongly suggested that microfibril formation through fibrillin-1 assembly plays an important role in PDL formation and function. However, the molecular mechanisms of fibrillin-1 microfibril assembly remain unclear as the microfibril-associated molecule that regulates or stabilizes fibrillin-1 microfibril formation has not yet been identified. Recent findings have revealed that ADAMSL6β is essential for the development and regeneration of the PDL through the direct interaction of fibrillin-1 to promote microfibril assembly [23,24]. These findings have also suggested that the administration of fibrillin-1 microfibrils provides a novel therapeutic strategy for the treatment of periodontal disease.

We here review the present status of the periodontal tissue regeneration technologies that focus on the molecular mechanisms underlying development, regeneration and tissue engineering of periodontal tissue, and also discuss the potential of ECM administration therapy through the promotion of microfibril assembly as a novel therapeutic strategy for the essential functional recovery of periodontal tissue.

2. Development processes in periodontal tissue

The PDL has essential roles in tooth support, homeostasis and repair, and is involved in the regulation of periodontal cellular activities such as cell proliferation, apoptosis, the secretion of extracellular matrices, resorption and repair of the root cementum and remodeling of the alveolar bone [25-27]. To develop future methods to regenerate damaged PDLs, it will be important to understand the molecular basis of PDL development.

2.1 Molecular mechanisms underlying periodontal tissue development

The PDL is derived from the dental follicle (DF), which is located within the outer mesenchymal cells of the tooth germ and can generate a range of periodontal tissues including

the PDL, cementum and alveolar bone [21]. The DF is formed during the cap stage of tooth germ development by an ecto-mesenchymal progenitor cell population originating from the cranial neural crest cells [28]. Given the critical role that the progenitor cell population in the DF appears to play in the development of periodontal tissue, the developmental processes in this tissue are of considerable interest in terms of further understanding the biology of these cells (Figure 1). The differentiation of the DF proceeds as follows: i) during the tooth root-forming stage, the Hertwig's epithelial root sheath (HERS) comprising the inner- and outer-dental epithelia that initiate tooth root dentin formation is fragmented into the Malassez epithelium resting on the tooth root surface; ii) the DF migrates to the surface of the tooth root and differentiates into cementoblasts to form the cementum matrix [29,30]; iii) at almost the same time, the DF differentiates into the PDL on the cementoblasts in order to insert collagen fibers, known as Sharpey's fibers, into the cementum matrix. Fiber insertion also takes place along the alveolar bone and iv) both bone- and PDL-derived fibers finally coalesce in the PDL to form the intermediate plexus, which resembles tendinous tissue [31-33].

The DF has long been considered to be a source of multi-potent stem cells (DFSCs), since these cells have the ability to migrate onto the tooth root surface to form periodontal tissue including cementum, PDL and alveolar bone during the tooth root-forming stage [32,34-37]. Previous studies have indicated that DF cells can form PDL-like tissues and cementum/bone-like structures after implantation into immunodeficient mice [38,39], supporting the notion that stem cells which can differentiate into PDL, cementoblast, osteoblast lineages are present in the DF [34,35]. To regenerate periodontal tissue, functional molecules which promote the differentiation of DFSCs into PDL need to be elucidated to enable a proper understanding of the mechanisms underlying periodontal tissue formation, including the pathways pertaining to PDL cell, cementum and alveolar bone differentiation.

2.2 Functional molecules involved in DF differentiation

Although the molecular mechanisms of DF development and differentiation remain to be determined, previous gene expression studies of mouse molar root development have suggested that some growth factors, including bone morphogenetic protein (BMP) 4, growth and differentiation factors (GDFs) 5, 6 and 7 [40-43], epidermal growth factors [44], *Shh* [45-47] and insulin-like growth factor (IGF)-1 [48], are involved in the growth or differentiation of the DF. Transcriptional factors such as *Scleraxis, Gli, Msx1, Msx2* and *Runx2* have also been shown to be involved in the differentiation of the DF into cementoblasts and in the mineralization of cementum [39,43,46,49]. Among these factors, GDFs and scleraxis are the most well characterized that are involved in tendon/ligament morphogenesis, suggesting that PDL development shares similar molecular mechanisms to those of tendon/ligament morphogenesis. With regard to

cementogenesis/osteogenesis of the DF, treatment of this tissue with BMP-2 and BMP-7 has been found to induce mineralization ability. In addition, previous findings suggest that PDL cells harbor mineralization inhibitory mechanisms that enable them to maintain a ligament structure across the mineralized tissue, including the alveolar bone and cementum, during PDL development [50-52]. These observations strongly suggest that the tendon/ligament-related cytokines, the BMPs, and inhibitors of mineralization are linked to the restoration of the tendinous structure of the PDL. The mechanisms involving these factors may also have a role in preventing ankylosis of the PDL.

3. Regeneration therapies for PDL defects

A partial restoration of periodontal tissue has been achieved previously using a guided tissue regeneration (GTR) technique which provides an adequate space and favorable niche for the repair of periodontal defects using barrier membrane [53]. From the results of these GTR therapies, regeneration of the PDL has been shown to be critical for recovering the connection between the cementum on the root surface and the alveolar bone.

To regenerate periodontal tissue that has been destroyed by periodontal disease requires the recruitment of PDL stem cells (PDLSCs) to properly reconstitute the PDL structure including its extracellular components such as the collagen and elastic fibril systems [32,33]. Recent studies of stem/progenitor cells have provided considerable new insights that have furthered our understanding of PDLSCs, which can differentiate into periodontal tissue cell lineages such as PDL, cementum and alveolar bone [14,54]. PDLSCs will have utility for the future development of stem cell transplantation therapies and tissue engineering applications to restore periodontal organ function as they replace damaged areas with enriched and purified stem cells and thereby achieve PDL repair (Figure 2) [14]. The biological potential of PDLSCs to stimulate the regeneration of periodontal tissue can now be realized by the local application of human recombinant cytokines.

3.1 Stem cell therapies

PDLSCs have been isolated from human PDL tissue by single-colony selection and magnetic activated cell sorting. PDLSCs express the mesenchymal stem cell markers STRO-1 and CD146/MUC18, and can differentiate into cementoblast-like cells, adipocytes and fibroblasts [14]. In addition, PDLSCs show the capacity to generate a cementum/PDL-like structure and contribute to periodontal tissue repair on transplantation into immunocompromised rodents. Clonal PDLSC analysis has further revealed that these cells show a similar phenotype to DFSCs since they also express *RUNX-2, Col I, ALP, OPN, OCN, RANKL, OPG, scleraxis, periostin, Col XII* and *alpha-SMA* mRNAs [54]. Importantly, PDL tissue collected from one tooth can give rise to many stem cells because of their high proliferation capacity *ex vivo*. Recently also, it has been shown that the transplantation of autologous PDLSCs obtained from the
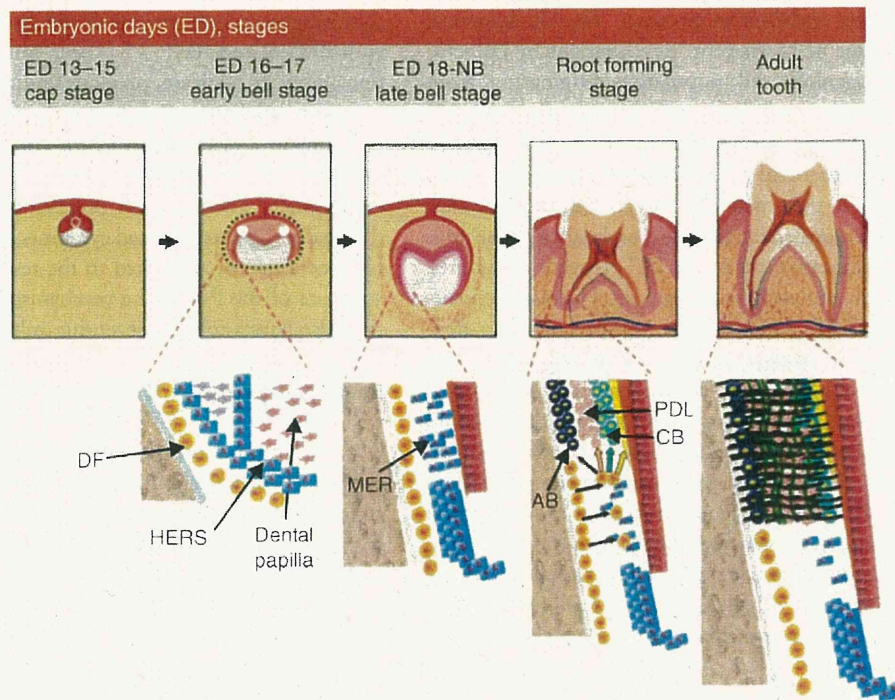
Figure 1. Developmental processes in the PDL (upper panel). PDL development originates from the DF located on the periphery of the tooth germ (arrows). The DF is generated from the dental mesenchyme during the cap stage of tooth germ development in the embryo. Development of the DF progresses during the early- and late-bell stages of the tooth germ, but no morphological changes are observed. Differentiation of the DF begins during the tooth root-forming stage and the mature PDL is subsequently formed (lower panel). DF differentiation commences after the tooth root dentin is formed by reciprocal interaction between the HERS and dental papilla. During tooth root dentin formation, the HERS is fragmented into the Malassez epithelial rest and the DF is then capable of migrating onto the root dentin to be differentiated into cementoblasts, PDL and alveolar bone to connect the tooth root and jaw bone (adult tooth).

PDL: Periodontal ligament; DF: Dental follicle; HERS: Hertwig's epithelial root sheath.

extracted teeth of miniature pigs can regenerate and repair a surgically created periodontal defect [55]. This finding suggests that PDLSCs obtained from an easily accessible tissue resource and expanded *ex vivo* using wisdom teeth might represent a feasible therapeutic approach to the reconstruction of tissues destroyed by periodontal disease.

In addition to the clinical application of stem cell transplantation, cell sheet engineering therapies for periodontal tissue regeneration are now being developed for clinical application [56,57]. In this technology, temperature-responsive dishes are used to harvest the cell sheets through a simple decrease in the temperature, thus avoiding the use of proteolytic enzymes [58]. The use of this method allows PDL cell sheets to be easily harvested and transplanted into periodontal defects *in vivo* [56,57,59,60]. PDL cell sheets have the potential to induce periodontal regeneration, including the reformation of the PDL and cementum. The available data also suggest that this technique has the appropriate efficacy for periodontal regeneration in patients with periodontal disease.

3.2 Cytokine therapies

Some new treatments that accelerate the regeneration of periodontal tissue by local application of human recombinant cytokines have now been established. This approach stimulates the proliferation and differentiation of stem cells/progenitors from the PDL into hard tissue-forming cells. The local application of human recombinant cytokines such as platelet-derived growth factor (PDGF) and IGF-1 [16,61], BMP-2 [62,63], TGF-β [64], osteogenic protein (OP)-1 [65] and brain-derived neurotrophic factor (BDNF) [66] stimulates and promotes the regeneration of regional periodontal tissue in animal models. The potency of PDGF-BB plus β-tricalcium phosphate (β-TCP, an osteoconductive scaffold) in periodontal tissue regeneration in human has also been recently reported [67]. In addition, a clinical Phase I study of fibroblast growth factor (FGF)-2 has shown that it stimulates the regeneration of periodontal tissue lost due to periodontal disease and demonstrated the safety of this treatment [15]. The results of this trial were clinically interpreted as a demonstration of